Morris, J.D., Villinger, H.W., and Klaus, A. (Eds.)
Proceedings of the Ocean Drilling Program, Scientific Results Volume 205

1. Leg 205 Synthesis: Subduction Fluxes and Fluid Flow across the Costa Rica Convergent Margin[1]

Julie D. Morris[2] and Heinrich W. Villinger[3]

ABSTRACT

Ocean Drilling Program (ODP) Leg 205 was designed to investigate subduction fluxes and fluid flow across the Costa Rica convergent margin. During Leg 205, modified CORK-IIs (new-generation Circulation Obviation Retrofit Kits) were installed within the incoming plate and the décollement zone to monitor pressure and temperature of formation fluids through time and to collect a time series of fluid samples for chemical analysis. One subseafloor observatory is monitoring within a highly fractured region of the incoming igneous section. Vigorous, slightly subhydrostatic flow within high-permeability horizons is observed; fluid compositions appear to be a mixture of bottom seawater and components distinct from seawater. The observatory within the décollement zone reveals pressures that are just slightly overpressured; excursions in the pressure and temperature record correlate temporally with excursions in fluid composition and flow rate variation, all occurring during periods of aseismic strain, recorded geodetically. Igneous and sedimentary core materials collected during Leg 205 have been studied extensively in combination with materials recovered during ODP Leg 170. This synthesis and papers in this volume report on the igneous and alteration history of the incoming oceanic section and its implications for off-axis magmatism and fluid flow, the composition of incoming and underthrust sediments with implications for fluid and element loss from the shallow subduction zone, the structure and permeability characteristics of the forearc sediment wedge, and the consequences of sediment dynamics and fluid flow to the seismogenic zone and subduction factory.

[1]Morris, J.D., and Villinger, H.W., 2006. Leg 205 synthesis: subduction fluxes and fluid flow across the Costa Rica convergent margin. *In* Morris, J.D., Villinger, H.W., and Klaus, A. (Eds.), *Proc. ODP, Sci. Results,* 205: College Station, TX (Ocean Drilling Program), 1–54. doi:10.2973/odp.proc.sr.205.201.2006
[2]Department of Earth and Planetary Sciences, Washington University, One Brookings Drive, CB 1169, St. Louis MO 63130-4899, USA. Present address: Division of Ocean Sciences, National Science Foundation, 4201 Wilson Boulevard, Arlington VA 22230, USA. **jdmorris@nsf.gov**
[3]FB Geowissenschaften, Universität Bremen, Postfach 330 440, 28334 Bremen, Germany.

Initial receipt: 14 March 2006
Acceptance: 23 August 2006
Web publication: 13 October 2006
Ms 205SR-201

INTRODUCTION

Fluid flow in convergent margins can have a profound effect on the shallow thermal structure of the downgoing plate, the physical properties of the subduction interface, and the transport of elements to the ocean, the volcanic arc, and the deeper mantle. It is, therefore, a major factor in understanding the impact of subduction zone processes on seismicity and, ultimately, volcanism at convergent margins.

Ocean Drilling Program (ODP) Legs 170 (Kimura, Silver, Blum, et al., 1997) and 205 (Morris, Villinger, Klaus, et al., 2003), and their post-cruise science, have investigated fluid flow across the Costa Rica margin, in the context of the lithology, structure, tectonics, and thermal history of the incoming plate, the overriding plate, and the décollement zone that separates them. During Leg 205 subseafloor observatories (CORKs: Circulation Obviation Retrofit Kits) were installed within fractured igneous rock of the incoming plate and in the décollement zone to monitor changing pressure and temperature of the formation fluids and to collect fluid samples for shore-based analysis. Data acquired to date represent the first high-resolution time series of combined pressure (P), temperature (T), chemical composition, and rates of fluid flow in the décollement of a subduction zone. Intriguing correlations between excursions in the fluid P, T, and composition records and aseismic strain events recorded geodetically set the stage for a long-term investigation into the role of fluids in seismogenic processes. The theme of fluid flow and long-term monitoring link many of the sections that follow.

Another major goal of the two legs was to characterize the mass and element fluxes, including volatiles, into the Middle America Trench, derived from both the altered oceanic basement and the sedimentary veneer. Coring during Leg 205 was restricted to specific target depths to maximize operational time for CORK installation. In conjunction with Leg 170, however, a large amount of cored sedimentary and igneous rock has been studied, with results reported here. During Leg 205, ~170 m of igneous rock was cored in the form of a ~30-m-thick gabbro sill separated from a lower igneous unit (>140 m thick) by intervening sediments. The lower unit also shows gabbroic textures, with chemical composition similar to ocean island basalt (OIB) in general and moderately enriched Galapagos lavas in particular. These results, together with studies in the literature, point to significant and extensive overprinting of the incoming oceanic plate by off-axis magmatism, likely related directly or indirectly to hotspot volcanism. Alteration is low overall but strongly concentrated along fractured horizons, including one that is the target of long-term monitoring.

This volume also reports results from the incoming and underthrust sediment sections. Comparison of equivalent sediment horizons cored on the incoming plate and from below the décollement sets the stage to investigate directly changes in sediment and pore fluid composition resulting from the initial compaction dewatering associated with the earliest stages of subduction. This is possible because Leg 170 showed no sediment accretion in the forearc and documented the sediment compaction associated with dewatering between the reference site on the incoming plate and the equivalent underthrust sediments. Several contributions discussed below address this topic.

The goals and accomplishments of Legs 170 and 205 nicely address objectives of those parts of the Integrated Ocean Drilling Program

(IODP) and MARGINS science plans that emphasize the seismogenic zone and the subduction factory. The seismogenic zone is that part of the convergent margin plate boundary where earthquakes occur on the interface between the two plates. The subduction factory refers to the contributions from the downgoing slab to the overlying plate (aqueous fluids, sediments, and hydrous melts) and their impact on fluid flow, hydrate formation, microbial activity, continent-building (and frequently explosive) volcanism, ore formation, and chemical modification of the deep mantle. Central America has been a high-priority region for both seismogenic zone and subduction factory studies. Correlated variations in sediment dynamics, seismicity, and volcanism along strike allow the linkages among them to be investigated. It is also one of the few active margins where a significant carbonate sedimentary section is being subducted, permitting investigation of CO_2 recycling in subduction zones. For the seismogenic zone, central questions involve the role of thermal structure, mineralogy, physical properties, and dehydration behavior of the subducting plate in controlling the onset of seismogenesis, all addressed by the two legs. The fate of underthrusting sediments and pore fluids, the composition and alteration of the igneous section of the incoming plate, and the advection of fluids from depth along the décollement, addressed here, all speak to issues important to the subduction factory as well as the seismogenic zone.

GEOLOGICAL AND GEOPHYSICAL BACKGROUND FOR ODP LEGS 170 AND 205

The general tectonic setting for Legs 170 and 205 is shown in Figure F1, and the bathymetry and topography of the margin are shown in Figure F2. Sites for the two legs were drilled across the deformation front outboard of the Nicoya Peninsula. Sites 1039 (Leg 170) and 1253 (Leg 205) penetrate the sedimentary and upper igneous sections of the incoming plate. They are located ~1 and 0.2 km, respectively, outboard of the deformation front. Holes 1040C and 1254A are located within 50 m of each other, ~1.5 km inboard of the deformation front. Both penetrate the forearc sediment prism and the décollement zone; coring in Hole 1040C recovered the entire underthrust sediment section and the top of a gabbro sill on the subducting plate. Sites 1043 and 1255 are again within 50 m of each other, ~0.4 km inboard of the deformation front. Both penetrated the sediment prism and the décollement zone. Leg 205 CORKs were installed at Sites 1253 and 1255. The lithology and structure of incoming and underthrust sediments are shown in Figure F3.

Incoming Oceanic Plate

The convergence rate of the Cocos plate relative to the Caribbean plate increases only slightly from 83 mm/yr offshore Guatemala to 85 mm/yr offshore Nicaragua, reaching 88 mm/yr offshore southernmost Costa Rica (DeMets et al., 1990). The convergence direction offshore the Nicoya Peninsula is almost perpendicular to the trench with the subducting plate dipping to the northeast (25°N–30°E). The maximum depth of seismicity gradually becomes shallower from Nicaragua (~200 km) to southern Costa Rica (~45 km). The dip angle of the slab in the upper 100 km is similar from Nicaragua to Central Costa Rica (~30°),

F1. Leg 205 bathymetry, p. 38.

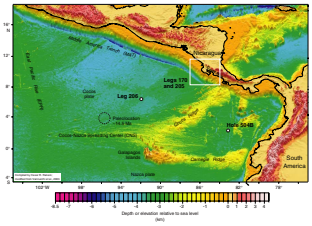

F2. MAT bathymetry, p. 39.

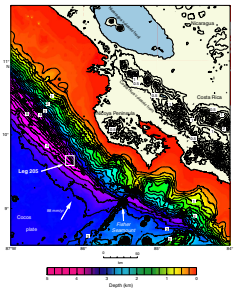

F3. Lithology summary, p. 40.

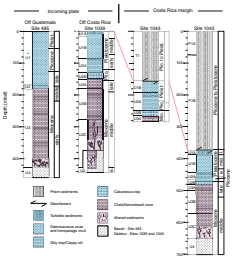

becoming steeper beneath Nicaragua at ~100 km depth, with a dip of ~80° (Protti et al., 1994).

There are significant variations in the origin and morphology of the incoming plate through the Nicaragua–Costa Rica segment of the Central American convergent margin (Figs. **F1, F2**). Large-scale tectonic features, such as the Carnegie and Cocos Ridges and the subduction trench, show up clearly in the regional bathymetry (Ranero et al., 2000a). Crust subducting beneath Nicaragua, formed at the East Pacific Rise (EPR), is pervasively faulted with offsets of up to 700 m on back-tilted normal faults (Kelly and Driscoll, 1998; Kelly, 2003), possibly associated with extensional tectonics caused by the flexure of the crust as it is subducted. The offsets become smaller moving south toward the vicinity of the Nicoya Peninsula, where they are <200 m. Farther southeast, seafloor relief in general is more pronounced (being southeast of the so-called "rough/smooth boundary" after Hey, 1977) and the seafloor is covered by numerous seamounts (Figs. **F1, F2**). Crustal thickness increases slightly from ~5 km offshore Nicaragua to ~6 km offshore the Nicoya Peninsula (Ranero and von Huene, 2000). The thickness of the incoming sediments is generally in the range of 400–500 m along the entire length of the margin (Fig. **F3**).

Analysis of marine magnetic measurements in Figure **F4** (Hey, 1977; Lonsdale and Klitgord, 1978; Barckhausen et al., 1998, 2001) shows that ~20 km southeast of the Leg 205 transect, a fracture zone trace (FZT) separates lithosphere formed at the EPR from that formed at the Cocos-Nazca spreading (CNS) center. This means that the drill holes of Leg 205 are underlain by crust that formed at the EPR at ~24 Ma. Wilson (1996) indicates that the crust at this location was formed at a full spreading rate of ~130 mm/yr. Seismic images of the FZT (Barckhausen et al., 2001) confirm the location of the boundary and reveal that the top of basement is ~100–200 m shallower on CNS-generated seafloor than on EPR-generated seafloor. The lithosphere southeast of the FZT formed at the CNS center, with decreasing age to the southeast. The oldest CNS crust abutting the FZT is 22.7 Ma, which corresponds to the breakup age of the Farallon plate. ODP Leg 206 Site 1256 (6°44.19′N, 91°56.06′W) is located on crust generated at the EPR at a full spreading rate of ~200 mm/yr in the immediate vicinity of the rough/smooth boundary (Fig. **F1**).

Seismic Profile BGR-99-44 (Fig. **F5**) reveals the general structure of the seaward side of the trench, the trench itself, and the toe of the forearc prism. All drill sites of Leg 205 are located on this multichannel seismic (MCS) line (C. Reichert and C. Ranero, pers. comm., 2001), shot in 1999. The data were acquired with a 6-km, 1024-channel digital streamer using a 3-m^3 tuned air gun array and differential Global Positioning System (GPS) navigation. Data shown in Figure **F5** are a near-trace (171-m offset) time-migrated section of the complete profile. The incoming pelagic sediments with a thickness of ~400 m show faults with offsets of 50–100 m seaward of the trench. A prominent reflector at 0.25 s two-way traveltime (TWT) below the seafloor marks the base of a late Miocene sedimentary unit. Beneath the sedimentary sequence, the strong reflection at 0.5 s (TWT below seafloor) images the top of a gabbro sill as revealed by drilling results from Leg 170 at Site 1039. The top of oceanic basement below the sill is very difficult if not impossible to identify based on the seismic records.

Heat flow data from the Global Heat Flow Database and from more detailed studies in the area (Langseth and Silver, 1996; Ruppel and Kinoshita, 2000; Fisher et al., 2003b; Hutnak et al., in press) reveal a clear

F4. Magnetic anomaly isochrons, p. 41.

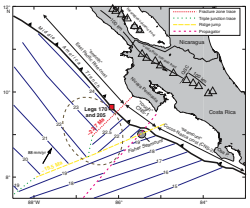

F5. MAT MCS profile, p. 42.

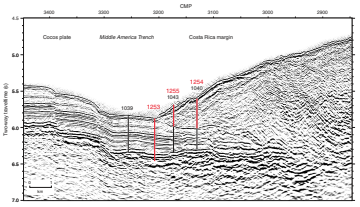

overall picture. North of the FZT, heat flow values average ~30 mW/m², about one-third of the conductive lithospheric value (Stein and Stein, 1992); values jump to an average of ~110 mW/m² south of the FZT, consistent with lithospheric cooling models. Given the similar plate age north and south of the FZT, these data imply that a substantial amount of heat is being removed by hydrothermal circulation within the EPR crust to the north. A detailed heat flow study prior to Leg 170, focusing on the trench and the prism offshore the Nicoya Peninsula (Langseth and Silver, 1996), confirmed the observation of a cool plate subducting under Costa Rica. Two more recent heat flow surveys (TicoFlux I and II) investigated in detail the thermal structure of the incoming plate seaward of the Leg 205 area by mapping heat flow along seismic lines (Fisher et al., 2003a, 2003b; Hutnak et al., 2006). Three major conclusions can be drawn:

1. Small and isolated areas show either very high or very low heat flow, usually associated with basement highs, indicative of active recharge or discharge.
2. Profiles across the FZT show locally an increase of heat flow but in general the transition is offset ~20–50 km from the FZT and depends on the proximity to outcrops, not to the tectonic boundary.
3. A profile seaward of the deepest part of the trench across major extensional faults shows no indication that these faults act as major fluid conduits.

New heat flow values at the prism from northern Nicaragua to southern Costa Rica (*Meteor* Cruise 54-2) clearly support the idea that there is a major thermal boundary in the vicinity of the FZT, not only seaward of the trench but also underneath the prism.

Forearc

Seismic data from the Costa Rica forearc and coring during Leg 170 (within 7 km of the trench) show that the bulk of the Pacific margin is a wedge-shaped high-velocity body probably made of rocks similar to the Nicoya ophiolite complex cropping out along the coast (Shipley et al., 1992; Kimura, Silver, Blum, et al., 1997; Ranero and von Huene, 2000). The proximity of the presumed ophiolitic basement to the trench precludes the existence of any significant sediment mass derived from recent accretion; only a small sediment prism (<10 km wide) is located at the front of the margin wedge. Initially, MCS images were interpreted in terms of sediment accretion to the Costa Rica margin (Shipley et al., 1992). More recently, however, and in the wake of Leg 170 drilling, seismic images have been interpreted to show that essentially the entire sediment cover of the ocean plate is currently underthrust beneath the margin and that the frontal sediment prism is storing very little, if any, of the incoming material (Kimura, Silver, Blum, et al., 1997; Christeson et al., 1999, 2000; McIntosh and Sen, 2000; Moritz et al., 2000; Silver et al., 2000; Ranero et al., 2000b; von Huene et al., 2000).

Part of the prism relevant to Leg 205 is imaged in the seismic line shown in Figure **F5.** Northeast of the deformation front (shotpoint 3210) the décollement is clearly visible as a boundary separating the underthrust sediment sequence from the overlying poorly structured prism sediments. Detailed analysis of a three-dimensional seismic data set (Shipley et al., 1992) shows that the décollement structure is quite

diverse across the lowermost part of the prism (within an 8.5 km transect). Shipley et al. (1992) were able to identify numerous thrust faults, mostly in the deeper part of the prism, possibly acting as fluid conduits, but clear tectonic structures are less evident approaching the deformation front. Only one of these faults is imaged offsetting the underthrust sequence (Fig. F5) (common midpoint 3155) and appears to continue up into the prism sediments.

As shown in Figure F3, the sediment section beneath the décollement at Site 1040 repeats the complete lithology and sequence of the incoming section cored at Site 1039, allowing little sediment accretion to the front of the prism at present (Kimura, Silver, Blum, et al., 1997). Cosmogenic ^{10}Be, which decays with a 1.5-m.y. half-life, also shows that little, if any, frontal accretion has taken place at this site over the last several million years (Morris et al., 2002). The sediment wedge is thus either a paleoaccretionary prism or is composed largely of slumped slope sediments rather than accreted marine sediments. Sedimentological and chemical data (Kimura, Silver, Blum, et al., 1997; Morris, Villinger, Klaus, et al., 2003) are more consistent with the latter interpretation.

The composition of arc lavas often records a sediment contribution from the downgoing plate, constraining sediment dynamics at depths greater than those that can be reached by drilling or seismic imaging. Chemical differences between the arc lavas from Nicaragua and Costa Rica suggest that the entire sediment section is subducting to the depths of magma generation beneath Nicaragua, with the carbonate section dominantly subducting beneath Costa Rica (Morris et al., 1990; Carr et al., 1990, 2003; Patino et al., 2000; Reagan et al., 1994). The seismic and lithologic observations indicate complete sediment subduction past the prism front in both regions. The arc and prism observations can be reconciled if sediments are underplated to the base of the prism beneath Costa Rica or if greatly enhanced subduction erosion occurs beneath the Nicoya segment. Christeson et al. (1999) used seismic reflection and refraction data to show stacked velocity duplicates, interpreted as repeated stratigraphic sections due to underplating beneath the deeper part of the Costa Rica prism.

In addition to evidence for sediment subduction and underplating beneath the Nicoya segment, the seismic stratigraphy and multibeam bathymetry of the slope offshore Nicaragua and the tectonic structure offshore Costa Rica indicate significant mass wasting and extension and subsidence of the margin during much of the Miocene (Ranero et al., 2000b; Ranero and von Huene, 2000; Walther et al., 2000; Clift and Vannucchi, 2004; Meschede et al., 1999), which is consistent with tectonic erosion and thinning of the overriding plate. These results are further substantiated by Leg 170 coring at Site 1042, located 7 km landward of the Middle America Trench, which encountered a ~30-m-thick sequence of fossiliferous well-lithified calcarenite breccia at a depth of ~4000 meters below sea level (mbsl) (Kimura, Silver, Blum, et al., 1997). Fossil, textural, cement paragenesis, and sedimentological observations document that the calcarenite was formed, brecciated, and cemented in a shallow nearshore setting (Vannucchi et al., 2001). Sr isotope ratios place the depositional age at ~16–17 Ma (latest early Miocene). It is overlain by ~320 m of unconsolidated slope mud showing the complete Pleistocene to Miocene sequence, where benthic foraminifers indicate the subsidence of the margin from the upper bathyal to abyssal depths (Meschede et al., 1999; Vannucchi et al., 2001). Unfortunately, erosion rates over the last several million years are less well con-

strained. Speculation is that tectonic erosion has been controlled by the roughness of the subducting plate. Thinning of the overriding plate and the continental margin morphology suggest that subduction erosion increases in intensity from Nicaragua to southern Costa Rica (Ranero and von Huene, 2000).

For the purposes of Leg 205, an important result is that the margin offshore Nicoya is not currently accreting sediments and has not done so over the last several million years. The conclusion that all sediments fed to the trench over this time frame have been subducted below Site 1254/1040 greatly simplifies estimating the mass and element fluxes in this shallow part of the system. Changes in underthrust sediment thickness between Sites 1039/1253 and 1040/1254 are due to compaction and dewatering in the earliest stages of subducting, with underplating playing a role farther downdip. Subduction erosion is likely to be an episodic rather than steady-state feature of the margin, as discussed below.

Hydrology across the Margin

Coring during Leg 170 and subsequent postcruise studies identified three distinct fluid flow systems. These included flow of modified seawater within the upper oceanic crust, lateral updip fluid flow within underthrust sediments, and fluid expulsion along the décollement and through faults in the margin wedge (e.g., Silver et al., 2000; Kastner et al., 2000; Saffer et al., 2000; Chan and Kastner, 2000).

The existence of fluid flow in the oceanic basement of the incoming plate (Site 1039/1253) is evidenced by both the heat flow anomalies discussed earlier and the chemistry of pore fluids sampled during Legs 170 and 205. Postcruise studies of pore fluid chemistry (Fig. **F6**) indicate that chemical characteristics typical of modern seawater are sampled in pore waters from the uppermost sediments. Deeper in the sediment section, values depart increasingly from seawater values as a result of diagenesis, largely ash alteration. The consequence is that measured pore fluid isotope ratios at a particular depth are lower than those of seawater at the comparable age, as determined from the paleoseawater Sr isotope curve. Pore fluid chemistry of the deepest sediments, however, trends back toward modern seawater values. Similar reversals in pore fluid chemical profiles at the base of the sedimentary section are seen for a wide variety of tracers (see fig. F20 in Shipboard Scientific Party, 2003). The heat flow anomaly and pore fluid profiles have been modeled in terms of lateral fluid flow in basement at rates of ~1–5 m/yr (Silver et al., 2000), with fluids having a residence time of at least ~15,000 yr. Thermal modeling from Fisher et al. (2003a) of the EPR segment is consistent with advective heat extraction in the uppermost 100–600 m of basement, with flow rates modeled in the range of 3–30 m/yr, suggestive of high-permeability horizons in the shallow part of the incoming plate, similar to that inferred for off-axis ridge flanks (Becker et al., 1997, 1998; Fisher, 1998; Davis et al., 2000; Kopf et al., 2000).

The décollement and faults cutting through the forearc sediment wedge of the upper plate serve as pathways for updip flow of fluids whose chemistry point to a source region with temperatures of 80°–150°C. Structural observations across the décollement (Fig. **F7**) indicate a zoned fault with heavily fractured fault rocks above a ductile plastic zone that may act as an aquitard, segregating the flow systems above and below the plate boundary (Vannucchi and Tobin, 2000; Tobin et al., 2001). At Sites 1040 and 1254, deformation increases gradually downward. Shipboard structural geologists placed the top of the dé-

F6. Pore fluid composition, p. 43.

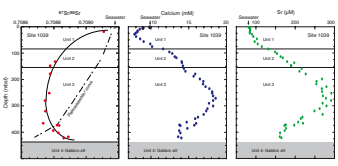

F7. Geochemical anomalies, p. 44.

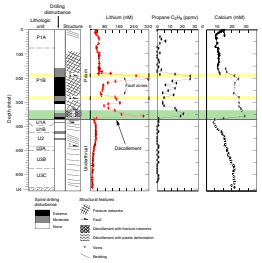

collement zone at 333 meters below seafloor (mbsf) and 338 mbsf at Sites 1040 and 1254, respectively. The base of the décollement is a sharp boundary at 371 and 368 mbsf at the two sites, respectively (see fig. F24 in Shipboard Scientific Party, 2003).

Pore fluid chemical profiles measured during and since Legs 170 and 205 at Site 1040 show three distinct intervals. Above ~190 mbsf, Li, propane, and Ca concentrations are relatively uniform, as they are again in the underthrust sediments below the décollement. Generally high Li, propane, and Ca concentrations are observed between ~200 mbsf and the décollement, with peaks typically coincident with fault zones. Similar chemical anomalies, albeit of smaller magnitude, are also seen along the décollement zone at Sites 1043 and 1255 (~130–150 mbsf). Enrichments in Ca and Sr, depletions in K, and changing Sr and Li isotopic compositions, as well as higher concentrations of thermogenic heavy hydrocarbons (propane to hexane), are also observed in these faulted horizons. Collectively, these data indicate that some fraction of the fluids sampled along these localized horizons is derived from depths great enough that temperatures are 80°–150°C. The chemical variations shown in Figure **F7** suggest that the zone between 200 and 370 mbsf is heavily infiltrated by fluids originating from a depth where temperatures are between 80° and 150°C; the sharp peaks at ~200 and 350–360 mbsf indicate that the anomalies are supported by relatively recent advective flow along the upper fault and the décollement.

Chemical and structural studies indicate a third hydrologic system, which drains fluids from the underthrust sediment section (Saffer et al., 2000, Saffer, 2003; Silver et al., 2000; Morris, Villinger, Klaus, et al., 2003). Abrupt changes in pore fluid chemistry (Fig. **F7**) across the décollement indicate that this drainage is not primarily into the décollement zone but rather is likely accommodated by lateral flow. More rapid drainage and greater compaction of the uppermost ~100 m (Units 1 and 2) than Unit 3 may result from (1) more abundant coarse-grained high-permeability ash layers that focus flow, (2) higher permeability within the hemipelagic sediments, or (3) significant permeability anisotropy within the hemipelagic sediments (Saffer et al., 2000; Saffer, 2003). Overall, hydrological and geological modeling (e.g., Saffer et al., 2000; Silver et al., 2000; Fisher et al., 2003a, 2003b) suggests relatively high permeabilities in the oceanic basement, décollement, and underthrusting section, with the décollement being locally more permeable than the underthrusting sediments. Leg 205 CORKs are monitoring fluid flow within the igneous section and the décollement zone.

OVERVIEW OF ODP LEG 170 AND 205 OPERATIONS

As noted, a high priority for Leg 205 was the installation of modified CORKs (CORK-II; for details see Morris, Villinger, Klaus, et al., 2003, and Jannasch et al., 2003) into the fluid flow systems of the Costa Rica margin, successfully accomplished at Site 1253 on the incoming plate and at Site 1255 in the prism. In both cases, drilled holes were cased with cement, with 4.5-in casing run in the hole to house sampling and pressure screens and the downhole instrumentation (see Morris, Villinger, Klaus, et al., 2003, for operational details). Postinstallation, a packer was inflated to isolate the horizon of interest from overlying levels. Installations at both sites monitor P and T of formation fluids at

selected intervals while simultaneously collecting a time series of inflowing fluids for subsequent analysis of dissolved and gaseous species (see Jannasch et al., 2003). Pressure monitoring follows the methods described in Davis et al. (2000), and methods of temperature monitoring are described in **Heesemann et al.** (this volume). The fluid samplers (OsmoSamplers) use osmotic pumps to suck fluid from the inlet ports and pump it into long, clean Teflon coils or copper coils (for later analysis of gaseous species), thus creating a time series of stored fluid. Redundant OsmoSamplers were deployed at every level instrumented.

Schematics in Figure **F8** show the design of the CORK at Site 1253, which is monitoring and sampling within a fractured region of the upper igneous section. At this site, a screen for pressure monitoring and fluid collection is located at a depth of 497–504 mbsf with a dangling OsmoSampler deployed at 512–519 mbsf. Miniature temperature loggers (Pfender and Villinger, 2002) are deployed with the OsmoSamplers at both levels. Both OsmoSamplers are within the open hole beneath a packer centered at 473 mbsf. Another screen for pressure monitoring is located just above the packer.

Several attempts to install a CORK-II with instrumentation in the décollement zone failed at Site 1254 (Morris, Villinger, Klaus, et al., 2003) but were successful at Site 1255. As shown in Figure **F9**, the sampling screen and one pressure screen are within the décollement, centered at a depth of 140.2 mbsf. The packer is located at 129.3 mbsf, and the hole ends at 153 mbsf, creating a very limited horizon around the décollement zone for fluid sampling. A second screen for monitoring pressure is again located just above the packer, and miniature temperature loggers are again deployed with the OsmoSamplers. Downhole instrumentation at Site 1255 also included an OsmoFlowmeter experiment (Jannasch et al., 2003). Located below the OsmoSamplers, the flow meters use osmotic pumps to inject a tracer fluid into the formation at a constant rate. Four sampling ports on the same horizontal plane as the injection port sample the formation fluid that has mixed with the injected tracer fluid. Dilution of the tracer is proportional to rate of fluid flow; azimuthal variation in the flow rate recorded in the four sampling ports speaks to anisotropy in the fluid flow. Unfortunately, the operations required to install the CORK and its instruments make it impossible to link flow directions as sampled by the OsmoFlowmeters to a geographic reference frame.

Despite the emphasis on downhole instrumentation, 370–600 mbsf was cored during Leg 205 at Site 1253 (equivalent to Leg 170 Site 1039) on the incoming plate. In addition to the sill and lower igneous complex discussed above, Leg 205 coring recovered, for the first time, sediments from the 30-m interval between the two igneous subunits. In the sedimentary wedge, Leg 205 cored from 150 to 223 mbsf and 300 to 368 mbsf in Hole 1254A, equivalent to Hole 1040C. Coring focused on an upper fault zone and the décollement zone itself, with penetration to the uppermost part of the underthrust sediment section. At Site 1255, equivalent to Site 1043, coring was limited to the interval about the décollement, 123–157 mbsf. Despite the limited coring, a significant amount of work is emerging from the papers in this *Scientific Results* volume, combining results for samples from Legs 170 and 205.

F8. Hole 1253A installation, p. 45.

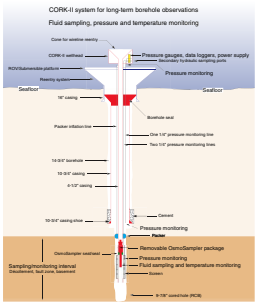

F9. Hole 1255A installation, p. 46.

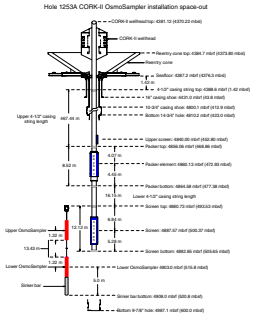

PRIMARY RESULTS OF ODP LEGS 170 AND 205 AND RELATED EXPERIMENTS

Igneous Petrology and Alteration History of the Subducting Plate

Approximately 170 m of igneous rock was cored during Leg 205 at Site 1253, with two primary objectives in mind. One was to use core descriptions and borehole logging to identify zones of higher alteration and fracture density within the drilled section, which would be targets for long-term monitoring. These horizons are candidates for localized fluid flow, which could be responsible for the significantly lower heat flow in the region and for the return to near-seawater compositions seen in basal sediment pore water profiles, discussed above. A second goal was to characterize the composition and alteration history of the igneous basement entering the Middle America Trench (MAT) to better constrain the flux of volatiles and other elements through the seismogenic zone and beyond to the depths of magma generation beneath the Central American volcanic arc (CAVA). This goal can be accomplished through a combination of Legs 205 and 206 (Wilson, Teagle, Acton, et al., 2003) and IODP Expeditions 309 and 312 (Teagle, Alt, Umino, Miyashita, Banerjee, Wilson, et al., in press). The latter three focused on deep drilling of the oceanic section at Site 1256 (see Fig. **F1**). This site is located along approximately the same flow line from the EPR to the MAT as is Site 1253. At Site 1253 itself, drilling bottomed in what proved to be a thick complex (>150 m) with chemical compositions typical of OIB rather than mid-ocean-ridge basalt (MORB). Leg 205 thus sampled a large amount of OIB overprinting on the subducting plate and can speak to its origin and significance but cannot address the nature of the crust generated at the EPR, or its alteration history.

Igneous Character and Origin of Leg 205 Gabbros

Igneous rocks were recovered at Site 1253 between ~400 and 430 mbsf (Subunit 4A) and from 450 mbsf to the bottom of the hole at 600 mbsf (Subunit 4B). As seen in Figure **F10,** Subunit 4A is clearly a sill, being relatively flat lying and bounded by sediments above and below. It is comparable to similar units cored in Leg 170 Holes 1039B and 1039C, drilled ~1 km seaward of Site 1253, and in Hole 1040C (Kimura, Silver, Blum, et al., 1997). Calcareous nannofossil dating of sediments above and below the sill indicates a minimum age for the sediment of 15.6 Ma and a maximum age of 18.2 Ma (**Muza,** this volume), implying sill emplacement more recently than 18.2 Ma and perhaps since 15.6 Ma. Carbon and oxygen isotope stratigraphy suggest that the age of these sediments may be <15.7 Ma (see **"Biostratigraphy,"** p. 14, and **Strasser et al.,** this volume). These younger ages are in contrast to the age of the Cocos plate in this vicinity, estimated at ~24 Ma, on the basis of marine magnetic anomalies (Barckhausen et al., 2001). The lower igneous complex (Subunit 4B) is composed of at least seven distinct petrologic units (Morris, Villinger, Klaus, et al., 2003). At all depths, recovered rocks include sparse microcrystalline intervals interspersed with more abundant fine- to medium-grained rocks with occasional coarse-grained horizons. True glassy horizons are extremely rare. Whether described as microgabbros, diabases, or gabbros, the textures of the cored rocks speak to generally slow cooling rates appropriate for large intruded bod-

F10. Hole 1253A petrology, p. 47.

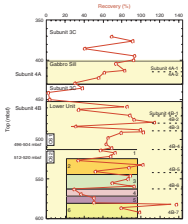

ies (formed by multiple magma injections in this case) or the deep interior of thick ponded lava flows. With extremely good recovery overall, and in the absence of almost any glassy selvages, we describe the lower unit as also being intrusive. Baked sediments at the top of Subunit 4B are in the same age bracket described by **Muza** (this volume) for Subunit 4A, implying similar ages for the two intrusive units. Radiometric dating is under way.

In terms of primary mineralogy and composition, the rocks from Subunits 4A and 4B are quite similar. They have abundant plagioclase and clinopyroxene phenocrysts, with ilmenite and magnetite microphenocrysts, often in a largely holocrystalline matrix; olivine and orthopyroxene phenocrysts occur rarely. Samples from Subunit 4A typically have higher concentrations of the more incompatible elements than do those from Subunit 4B, at comparable Mg numbers. Similarly, postcruise work (**Dreyer et al.,** this volume) shows that samples from Subunit 4A have higher rare earth element (REE) concentrations and slightly steeper REE patterns than do samples from Subunit 4B, although all have relatively flat heavy REE (HREE) patterns. These two geochemical groupings are also seen in the rocks recovered from Leg 170, although they were not identified at the time.

Nd isotopic work by Chavagnac, reported in **Dreyer et al.** (this volume), shows a very restricted range of composition (atom ratios of 0.51293–0.51299, with one sample at ~0.51304), which is important in several regards. Samples from Subunit 4A overlap with those from Subunit 4B, indicating that the differences in element concentrations just discussed are mostly, although not entirely, the result of variations in extent of partial melting and crystal fractionation. The Leg 205 samples have isotopic ratios lower than typical for MORB but similar to OIB values in general and to a subset of Galápagos lavas in particular. Lavas erupted above the Galapagos plume show a wide range of chemical variation and have been characterized as the result of mixing between a depleted MORB mantle (DMM, presumably entrained upper mantle) and plume components. Following Harpp and White (2001) those plume components can include what is inferred to be a long-term enriched lower mantle (PLUME), an incompatible trace element enriched mantle (FLO), and a high U/Pb mantle with elevated Pb isotope ratios (sampled along the so-called Wolf-Darwin lineament). As shown in figure F10 in **Dreyer et al.** (this volume), samples from other off-axis volcanism in the region (e.g., Fisher Seamount and Cocos-track tholeiites) have either similar isotopic compositions (Fisher) or a wider range of variation encompassing that shown by the Leg 205 samples. The Nd isotopic composition of the mantle source for the Leg 205 samples can be generated by mixing 30%–50% DMM with 50%–70% enriched Galápagos plume mantle (PLUME). There is a hint of a possible FLO contribution to gabbros sampled from Leg 170, Subunit 4A (see **Dreyer et al.,** this volume), although this could also be the consequences of seafloor alteration. Pb isotopic analyses are under way to further test these identifications and mixing models and to test for the presence of the high U/Pb contribution seen in the Wolf-Darwin lineament (Harpp and White, 2001).

Dreyer et al. (this volume) also use geochemical ratios such as La/Sm and Hf/Ta, which are little affected by varying amounts of crystal fractionation, to constrain mantle melting models for the Leg 205 samples. When using the mixture of enriched and depleted mantle sources calculated from the Nd isotopic results, trace element modeling suggests 2%–7% partial melting to form the Leg 205 samples, with Subunit 4A

formed from lower degrees of melting than Subunit 4B. The gentle slope of the REE patterns at the HREE end indicate that little if any mantle melting occurred at depths of garnet stability (>60 km), in contrast to models for the majority of the Galápagos Islands, Galápagos Seamounts, and the aseismic Cocos and Carnegie Ridges (White et al., 1993; Hauff et al., 1997; Harpp and White, 2001). Constraints imposed by Nd isotopic compositions, trace element ratios, and REE abundances and patterns are simultaneously satisfied by models that mix depleted and enriched mantles as solids followed by melting; the timing of melting subsequent to mantle mixing is not constrained by the data.

Significant magmatism is present in this section of the Cocos plate, away from the ridges and hotspot tracks. As shown in Figure F4, the incoming plate just south of the Leg 205 sites is described as a seamount province; Fisher Seamount, at 14 Ma, is the northernmost of these. Using the regional distribution of a high-amplitude seismic reflector, which correlates with drilled gabbro sills at ODP Sites 1039, 1040, and 1253, Silver et al. (2004) propose a widespread area of sill intrusion at ~8–10 Ma. Based on results to date for the Leg 205 samples, the modeling suggests upwelling of enriched mantle to depths shallower than 60 km and extensive mixing with ambient depleted upper mantle. This mixed mantle is melted at some later time to produce the lavas erupting at the surface. If additional isotopic work currently under way shows that this upwelling mantle is indeed similar to that of the Galápagos hotspot, then significant input of enriched mantle is seen at distances several hundred kilometers beyond the surface expression of typical hotspot activity. Speculation is that ridge jumps at ~22.7 and 19.5 Ma may have facilitated more distal emplacement of enriched mantle (e.g., Barckhausen et al., 2001) The presence of 14-Ma and perhaps 8- to 10-Ma igneous rock in the region suggests that later events in the plate history trigger melting. One possibility is that decompression melting could be related to a changing stress regime as the site approaches the trench or as the Cocos Ridge intersected the MAT (Silver et al., 2004; Abratis and Woerner, 2001). A speculative alternative is that serpentinization of the mantle of the incoming plate (e.g., Hacker et al., 2003) outboard of the trench could help lower melting temperatures locally. Preexisting zones of weakness in the lithosphere, resulting from prior plate rearrangements, could then provide conduits for magma emplacement. Detailed consideration of paleolocations and forthcoming ages for the Leg 205 rocks will aid this debate.

Alteration of the Cored Section

Alteration in Subunits 4A and 4B is generally low in abundance (1–5 vol%), except at specific horizons (Morris, Villinger, Klaus, et al., 2003). Within the upper sill, alteration is characterized primarily by palagonitization of glass in the groundmass and in veins and primary mineral replacement (most olivine and typically 10% of plagioclase phenocrysts) with clay minerals (saponite and, rarely, a chlorite-group clay). Voids and veins, typically <1 mm wide, are primarily filled by clay with minor zeolites. In the lower igneous subunit, alteration is generally more abundant, particularly below ~509 mbsf. Clay (saponite, a chlorite-group clay, and possibly nontronite) replacement of glass, olivine, and plagioclase is more typically 10%–20% and may be locally as high as 50%. Zeolites are found filling voids and veins. Above ~509 mbsf, the zeolites are laumontite, mesolite, thomsonite, and scolecite. Only below this depth are phillipsite and stilbite identified. Calcite is

also present in veins in the lower subunit. A lack of oxyhydroxides and only very minor presence of celadonite could be related to more reducing conditions.

In addition to being more altered, Subunit 4B is also more fractured below ~509 mbsf (Fig. F11). Also below this depth, Formation MicroScanner images show more closely spaced conductive features that are continuous across all four pads at specific horizons (e.g., 513 mbsf). Pfender and Villinger (this volume) use Stoneley wave data from the Dipole Shear Sonic tool used in logging Hole 1253A to identify regions of energy loss in borehole sections with relatively smooth walls. These horizons of reduced Stoneley wave energy are good candidates for high-permeability regions and higher fracture density and correspond well to regions of high fracture density observed in the cores. Based on their analysis, they proposed that fluid flow in the igneous section is most likely at depths of ~468, 492, 500, 508, and 518 mbsf.

F11. FMS fracture distribution, p. 48.

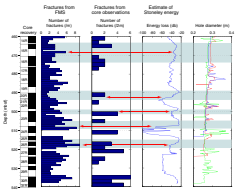

Strontium isotope data from Chavagnac for bulk rock samples (Dreyer et al., 2005) further show that significant alteration is restricted to specific horizons. Figure F12 shows that Sr isotope compositions for the Leg 205 samples are generally in the range of 0.7033–0.7035, values that are higher than those of MORB but within the range shown by OIBs (Zindler and Hart 1986). However, pronounced excursions to elevated Sr isotopic ratios (as high as 0.705) are observed at restricted horizons (~10–20 m wide) including those at ~513 and 565 mbsf. Increased uptake of elements such as Cs and Li are also observed at these depths. Slight shifts in Sr isotopic ratios are seen at shallower levels. Following the methods of Albarede (2003), Dreyer et al. (2005) calculated that a seawater:rock ratio of ~6 was necessary to produce the extreme shifts in Sr isotopic composition. The modeling further suggests that the fluids responsible for alteration are modified from modern seawater compositions as a result of their residence time in, and previous interactions with, the igneous section.

F12. Sr isotope stratigraphy, p. 49.

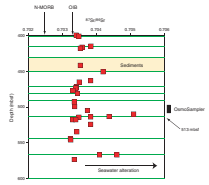

The coring, logging, and chemical data suggesting localized intervals for fluid flow are particularly interesting in combination with heat flow data from this region, which averages ~30% of the value appropriate for the plate age and is locally as low as 1% of predicted near the Leg 205 sites and more typically 10%–15% in the vicinity of the drill sites (Langseth and Silver, 1996; Fisher, 2003a, Hutnak et al., 2006). Modeling of both thermal and chemical data suggest vigorous flow of cold fluids through high-permeability horizons in the subducting plate. Not clear is the hydrologic relationship, if any, between the thermal anomaly and the sills. The thermal anomaly is a large regional feature which likely extends beyond the region of sills inferred from seismic imaging and drilling (Langseth and Silver 1996; Silver et al., 2004), although it is greatest in the vicinity of the trench, in the region studied during Legs 170 and 205.

Implications for the Seismogenic Zone and the Subduction Factory

Although not successful in recovering EPR-generated basement of the incoming plate, the results from Leg 205 do have implications for the seismogenic zone and subduction factory. Modeling of thermal contours on the subducting plate shows that equivalent isotherms are shallower on EPR crust than on the adjoining CNS crust (i.e., the thermal perturbations caused by flow of cold fluid through the EPR seg-

ment may persist to significant depth and could affect seismogenesis) (Newman et al., 2002; Hacker et al., 2003; Spinelli and Saffer, 2004).

Significant OIB (?Galápagos) overprinting of the incoming EPR crust is important for understanding the flux of mass and elements into the subduction zone and to the depths of magma generation. It is not currently possible to arrive at any reasonable mass balance between MORB and OIB in the downgoing plate. Additional analysis of MCS data (e.g., Silver et al., 2004) in light of drilling results and improved velocity models may provide better constraints. However, we do know that the uppermost part of the incoming igneous section, over perhaps large areas, is composed of rocks with higher abundances of many trace elements (e.g., K, Rb, Cs, Sr, Ba, U, Pb, B, Li, and Be) than is typical of MORB. These shallowest igneous rocks, subjected to higher temperatures during subduction than are rocks deeper within the slab, also have more enriched isotopic compositions. Moreover, the localization of clays, zeolites, and calcites on preferred alteration horizons may make these intervals particularly susceptible to dehydration reactions, which generate fluids that move from slab to the mantle wedge and contribute to mantle melting and magma generation. Although we are not able to predict precisely how high-permeability horizons in the incoming plate would transform during subduction, it is conceivable that they could play a role in fluid transport from the slab to the upper plate across a wide range of depths.

Implications for Long-Term Monitoring

Figure F8 shows that the OsmoSamplers deployed during Leg 205 are located at depths of 497–504 and 512–519 mbsf. They are both within the open hole beneath a packer centered at 473 mbsf. They are thus well positioned to capture fluids inferred to flow along localized horizons, from both the Stoneley wave interpretations and the Sr isotopic results. Mixing of fluids from different horizons in the open hole will certainly occur, meaning that compositions of fluids in the samplers cannot be associated with unique horizons. In recovered fluids, any departure of compositions from seawater values would, however, contain indirect information about fluid-rock reactions in the oceanic crust.

Biostratigraphy

With an emphasis on installing subseafloor observatories, Leg 205 cored only at selected horizons. Samples and results from Legs 170 and 205 together, however, provide a good stratigraphic framework. Figure F3 provides a general overview of the stratigraphy of the oceanic sediment section as sampled on the incoming plate at Sites 1039 and 1253. It also shows the repeated sediment section beneath the décollement at Site 1043 (Site 1255) and Site 1040 (Site 1254), along with the lithology of the sedimentary wedge above the décollement. Results following Leg 170 highlighted the poor age control in the basal sedimentary section on the incoming plate and in the prism above the décollement, both of which are discussed here.

Age Constraints and Accumulation Rates for Mid-Miocene Carbonates

Leg 170 shipboard and postcruise biostratigraphic work at Site 1039 (Ibaraki, 2000; White, 2000; Muza, 2000) show very limited age control

through the middle Miocene carbonate section (between ~250 and 350 mbsf). Using Leg 205 coring, approximately one sample per cored sediment section from Site 1253 was analyzed biostratigraphically (**Muza,** this volume). High abundances and good preservation were typical for this site, except for samples nearest the igneous intrusions, which were either barren or highly recrystallized. Fossil assemblages in sediments both above and below the sill correspond to Martini's (1971) nannofossil Zone NN4, which has a minimum age of 15.6 Ma and a maximum of 18.2 Ma (Berggren et al., 1995), spanning the early/middle Miocene boundary. This same time bracket applies to the baked sediments located just above igneous Subunit 4B.

Strasser et al. (this volume, their fig. F8) point out a large discrepancy between biostratigraphic and magnetostratigraphic age estimates and accumulation rates through the middle Miocene. At a depth of ~360 mbsf, diatom, nannofossil, and foraminifer datums generally agree with each other, with age estimates from ~15.8 to 16.2 Ma as shown in the compilation in **Strasser et al.** (this volume). Interpolation between biostratigraphic datums suggests ages of 14–16 Ma at depths of 250–350 mbsf. As these same depths, however, magnetostratigraphic ages are 12–14 Ma. Figure **F13** shows bulk sediment carbon isotope stratigraphy for Site 1039 (a companion oxygen isotope stratigraphy is shown in **Strasser et al.,** this volume, their fig. F7), where $\delta^{13}C$ maxima are matched to the carbon isotope maxima CM 1–CM 6 from Woodruff and Savin (1991) and John et al. (2003). The carbon and oxygen isotope stratigraphies provide age constraints through the interval that has little or no biostratigraphic control. All isotopic age picks fall along an age-depth curve derived by interpolating between the biostratigraphic ages from above 250 mbsf and below 350 mbsf. They are thus consistent with sedimentation rates in the middle Miocene carbonate-rich Subunits U3B and U3C being approximately constant at ~50 m/m.y. This contrasts with the magnetostratigraphic estimates that suggest rates of ~18 m/m.y. between 16 and 13 Ma, with much higher rates at ~12.7 Ma. Note that the magnetostratigraphy could have been reset by sediment heating associated with sill emplacement.

F13. Carbon isotope stratigraphy, p. 50.

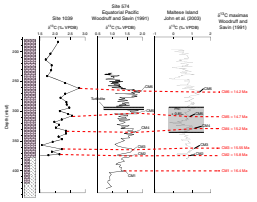

Constraints on Sill Emplacement

In addition to constraining sedimentation rates, the isotope stratigraphy also tightens age estimates for sill emplacement. Calcareous nannofossils from just above and below the sill yield the same age bracket of 15.6–18.2 Ma (**Muza,** this volume). A sample from a few meters above the sill in Hole 1039B is identified as CM 2 (= 15.8 Ma) and $\delta^{18}O$ Event B (15.75 Ma), suggesting that the younger age of the nannofossil bracket may be appropriate. Subunit 4A, with clear evidence for intrusion into the Miocene carbonate sediments, is thus likely younger than 15.8 Ma. Radiometric dating for the gabbro sill is under way and will test this interpretation. Radiometric ages will show whether sill intrusion here is associated with ~14-Ma volcanism as at Fisher Seamount or an 8- to 10-Ma event proposed by Silver et al. (2004). Dating is also in progress for the multiple sections within the lower Subunit 4B, to define the age spectrum for this lower igneous section. Once in hand, these ages relative to those of the overlying sediments should constrain the current interpretation of the lower subunit as an intrusive event and its temporal relationship to other magmatic events in the region.

Age of the Forearc Sediment Wedge

Age control for forearc sediments above the décollement was extremely difficult using samples from Leg 170 and generally remains so following Leg 205. This difficulty results from sparse abundance of nannofossils, poor preservation, and mixed species of different ages, consistent with a slumping origin for the prism sediments. In Hole 1254A, however, nannofossil assemblages are more diverse and generally more abundant than at Site 1040, especially within the upper cored interval (151–222 mbsf) and between ~351 and 359 mbsf. Although a precise nannofossil zonation for Site 1254 is not possible, **Muza** (this volume) offers a tentative biostratigraphy. His work suggests that sediments between 150 and 161 mbsf are of early Pleistocene age, sediments between 161 and 216 mbsf are late Pliocene, and those from 219 to 222 mbsf are early Pliocene, being no younger that 3.75 Ma. The lack of marker fossils in most of the sediments in the décollement zone precludes age determinations, but sediments from ~352 to 360 mbsf are early Pliocene in age but no younger than 3.75 Ma. Profiles of ^{10}Be vs. depth provide indirect age constraints (Morris et al., 2002), due to the ^{10}Be half-life of 1.5 m.y. As shown in that paper and Morris, Villinger, Klaus, et al. (2003), incoming sediments outboard of the trench and those below the décollement have very high ^{10}Be concentrations typical of marine sediments. Sediments above the décollement have uniformly low ^{10}Be concentrations, consistent with the particles being older than 3–5 Ma.

Geochemistry, Sedimentology, and Biogeochemistry

Leg 205 piggybacked extensively on the stratigraphy from Leg 170, shown in Figure **F3** (Kimura, Silver, Blum, et al., 1997; Silver, Kimura and Shipley, 2001). Despite the limited coring during Leg 205, a significant amount of geochemistry, sedimentology, and biogeochemistry is emerging from the papers in this volume, combining results for samples from both legs.

Metalliferous Sediments on the Incoming Plate

Basal metalliferous sediments were identified above the gabbro sill (Subunit 4A) at Sites 1039 and 1253 on the incoming plate and in the underthrust section at Site 1040, in the sedimentary prism. At Site 1039, liesegang structures and other visual indicators of hydrothermal fluid flow were noted; enrichments of trace elements such as Cu, Ni, Zn, and V were observed for at least 50 m above the sill (Kimura, Silver, Blum, et al., 1997).

At Site 1253, visual indicators of hydrothermal activity were absent, but chemical signatures are clear. **Chavagnac et al.** (this volume) use the Ti/Al ratio to show that the bulk of carbonates cored during Leg 205 from Subunit U3C, both above the sill and below it, have similar if not identical detrital sources and proportions. With that established, these authors use the metalliferous index (MI = 100 × Al/Al + Fe + Mn) to assess the major element signature of hydrothermal enrichment. Deep-sea pelagic clays of the Miocene typically have MI > 51 (Kyte et al., 1993), with metalliferous sediments from the EPR and Juan de Fuca Ridge having much lower values, typically 1–10 (German et al., 1997, 1999). The Leg 205 Miocene carbonates show a wide range of MI, from

3.6 to 51.6, with a majority between 24 and 43; lowest values are typically closest to the igneous rocks. Concentrations of metals such as Cu, Co, Zn, Fe, V, and Ti are typically 2–3 times the values measured in background carbonates away from the igneous units, comparable with results from Leg 170.

It is likely that the metal enrichments seen in the basal sediments were imparted soon after sill emplacement, given that the most extreme metal enrichments are typical of those seen in hydrothermal systems. If so, the signature would be unrelated to the reversal in gradient seen in many aspects of the pore water chemistry discussed earlier. These reversals, which generally show a return toward compositions of modern seawater in the basal 120 m, would diffuse away if unsupported by flow in the last 15,000 yr (Silver et al., 2000). There is a hint that hydrothermal activity that affected the sediments can have minor impact on their associated pore fluids, in that Mn concentrations just above and below the sill are about 3 times those measured 30 m above the sill (Morris, Villinger, Klaus, et al., 2003). Sr isotope compositions in the pore fluids just above the sill, however, show no trend or deflection toward values typical of the gabbros, limiting the extent of recent interaction with hydrothermal fluids.

Tephra Chemistry, Arc Evolution, and Sediment Dynamics

Legs 170 and 205 cored abundant ash horizons throughout the entire section. Basal ashes, estimated to be ~15 Ma from biostratigraphy, have chemical characteristics typical of OIB lavas and may reflect explosive activity from the Galapagos hotspot. Clift et al. (2005) focus on chemical analysis of tephra from air fall ash horizons younger than 2.5 Ma to study evolution of the CAVA. The younger age of the tephra makes them less vulnerable to alteration, and all samples in their study were visibly unaltered. Tephra chemistry from cored ash deposits frequently allows study of the largest explosive eruptions and permits the history of arc volcanism to be read further back in time than is easily feasible in land-based studies and with age constraints from biostratigraphy. Direct correlation between tephra and lava chemistry is generally quite difficult, however, in that most lava studies focus on the more mafic eruptives and most tephras are from magma chambers that have evolved to very silicic compositions.

With that caveat clearly in mind, Clift et al. (2005) use tephra chemistry to look at temporal evolution in the CAVA and its link to the balance between sediment subduction and forearc erosion through time. In order to do this, they first use the generally tholeiitic character of the tephras, together with their light REE (LREE) abundances and patterns, to propose that the bulk of the ashes are derived largely from Costa Rica and possibly Nicaragua, rather than Panama.

In considering temporal evolution, several features stand out. The youngest ashes are the most mafic of the entire section. Whether this reflects a trend toward more mafic compositions in the last 15,000 yr or the increased likeliness of depositing more mafic ashes as the incoming plate approaches nearest the trench and arc is unclear. At ~1.45 Ma, an ash horizon is characterized by the lowest Nd isotope ratios and highest δ^7Li yet measured for the CAVA, best explained by large amounts of sediment subduction and recycling to the arc, significantly higher than that recorded by either older or younger ashes (Clift et al., 2005). Ashes from 1.45 Ma to ~250 ka have δ^7Li that are still elevated above values for modern CAVA lavas (Chan et al., 1999, 2002), seen even for bulk te-

phra samples that were acid washed prior to analysis. Clift et al. (2005) use the detailed Nd-Li isotopic systematics of the ashes to argue that a third component is needed in magmagenesis, in addition to depleted MORB mantle and subducted sediments. This third component must have high εNd and high δ^7Li, like either extremely altered subducted oceanic basalt crust or, as likely for the Nicoya ophiolite complex, which makes up the forearc basement (McIntosh et al., 1993; Kimura Silver, Blum, et al., 1997). In the latter case, tectonic erosion of the forearc basement (e.g., Ranero et al., 2000b; Vannucchi et al., 2001, 2003; Meschede et al., 1999; Clift and Vannucchi, 2004) could deliver materials of the right composition to the depths of magma generation. Recent Costa Rican lavas and the youngest tephras show evidence for a much smaller subducted component than seen in the older ashes (Carr et al., 1990; Patino et al., 2000; Carr et al., 2003; Morris et al., 1990), even though active forearc erosion has been imaged along the Costa Rica–Nicaragua margin. Consideration of the tectonic evidence together with the arc geochemistry suggests that periods of enhanced sediment subduction and subduction erosion may be episodic rather than steady-state features of the margin, perhaps engendered by seamount subduction (von Huene and Scholl, 1991; Morris and Ryan, 2003; Clift et al., 2005).

Pore Fluid Chemistry and Fluid Flow

Pore fluid chemistry determined for samples from Legs 170 and 205 is useful in a number of different ways. At each site (1039/1253, 1043/1255, and 1040/1254), the compositions place constraints on local diagenetic reactions that change pore fluid chemistry, as well as on the larger fluid flow systems affecting each region, as discussed above. Comparison of pore fluid profiles, gradients, and concentrations for selected species between the incoming plate and the prism sites also illuminates the character of the deeply sourced fluid, thought to have advected from depths where temperatures are in excess of 80°–90°C and perhaps higher. They also constrain the fluid-mobile behavior at shallow levels of elements such as Li, Ba, Rb, and Cs, frequently used as important tracers for understanding sediment recycling in volcanic arcs. In the absence of firm constraints otherwise, such treatments in the literature typically assume that the composition of sediments delivered to the depths of magma generation is that subducted beneath the trench, a topic investigated here and in the following section. Numerical modeling of reactive transport, using selected aspects of pore fluid compositions, also provides estimates of flow rates and fluid residence times, linking to the hydrology of the margin. All set the stage for later discussion of long-term monitoring.

Solomon et al. (this volume) investigate changes in pore water Ba and sulfate between the incoming and underthrust sections. Ba in marine sediments may be tied up in barite ($BaSO_4$), other biogenic phases such as refractory organic matter and carbonate, or inorganic phases such as detrital silicates and Fe-Mn oxides and oxyhydroxides. Ba in aluminosilicates is generally regarded as immobile during diagenesis, but Ba in barite is strongly affected by pore fluid sulfate concentrations (Dymond et al., 1992, 1996; McManus et al., 1998; Torres et al., 1996b). Depletion of pore fluid sulfate via microbially mediated oxidation of organic carbon or methane can greatly increase the solubility of barite, and dissolved Ba^{2+} concentrations can increase by several orders of magnitude (Brumsack and Geiskes, 1983; Torres et al., 1996a; Dickens,

2001). Figure F14C and F14D show that the uppermost part of the incoming sediment section (with 13–25 mM SO_4^{2-} at Site 1039) undergoes sulfate depletion during earliest subduction (SO_4^{2-} = 0 in the upper 30 m of the underthrust section at Site 1040/1254). **Solomon et al.** (this volume) suggest that initial underthrusting severed the supply of sulfate from seawater to surface sediment via diffusion. In the ~17 k.y. required to move between the two sites, sulfate-reducing bacteria utilized the pore fluid SO_4^{2-} in the upper 30 m, depleting it to zero. This zero pore fluid sulfate horizon would presumably deepen with increasing time and downdip subduction. Figure F14A and F14B shows changes in Ba concentrations in pore fluids in the uppermost sediments between the incoming and underthrust sections. These changes are strikingly complementary to those seen in the sulfate profiles. Where pore fluid sulfate has not been exhausted, Ba pore fluid concentrations are similar at comparable depths in the incoming and underthrust sections. Where pore fluid sulfate concentrations have dropped to zero in the underthrust section, Ba pore fluid concentrations have increased by a factor of ~50 over comparable depths in the incoming section. As the zero sulfate zone progresses downward during subduction, Ba would be liberated from greater depths in the subducting sediment section.

Haeckel (this volume) models the downward propagation of the zero sulfate zone shown in Figure F14 using measured methane and sulfate concentrations above and below the décollement, measured porosity data, and an anaerobic methane oxidation reaction. In the ~17-k.y. time step since the underthrust section passed below the deformation front, Haeckel estimates that 1264 mol/m² of methane is oxidized by the reaction, equivalent to ~15 kg/m² of carbon. The model predicts a barite dissolution rate of 1.2×10^{-5} mM/yr, equivalent to a Ba^{2+} flux of 4025 mol/m² and sulfur dissolution of 130 kg/m² in the 17 k.y. of earliest subduction.

Kastner et al. (this volume) expand the spectrum of elements measured in pore fluids from the incoming and underthrust sediments and add Sr, Li, and Cl isotope measurements to the data set. Sr isotope ratios measured from basal carbonates on the incoming plate, cored during Leg 205, show the same trend seen in Leg 170 pore fluids and discussed earlier. Pore fluids in basal sediments show a shift toward higher $^{87}Sr/^{86}Sr$ values, intermediate between modern seawater and Miocene seawater ratios (see also **Kastner et al.,** this volume, their fig. F4A). Li isotope ratios in basal carbonates show similar systematics, as do profiles for Ca^{2+}, Sr^{2+}, Li^{+}, NH_4^{+}, PO_4^{3-}, alkalinity, and sulfate (Morris, Villinger, Klaus, et al., 2003). Higher Ca concentrations in pore fluids from the basal carbonates are observed relative to pore fluids from higher in the carbonate section; there is a general but not perfect tendency for pore fluid Ca and F concentrations to covary positively. As noted previously, these gradients indicate recent to contemporaneous fluid flow (Kastner et al., 2000; Silver et al., 2000).

Haeckel (this volume) uses reactive transport modeling of sulfate, ammonium, and phosphate profiles vs. depth to investigate two models that could support the gradients seen in the basal pore fluids. One invokes upward advection of distinctive pore fluids through the basal sedimentary section just above the sill. The other envisions lateral fluid flow in the basement, with upward diffusion of solutes through the basal sediments. As the author notes, the models are strongly dependent on the sulfate profile assumed as a starting condition. An advective model can fit the observed data across a wide range of initial sulfate

F14. Ba and sulfate contents, p. 51.

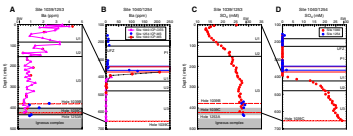

conditions. The best fit to the observed profiles is met with a vertical fluid velocity of 0.15 cm/yr for the past 200–240 k.y., which seems hydrologically unlikely for reasons discussed below. A diffusive transport model can fit the data if the system has been running for ~1 m.y. and if pore fluids through the entire sediment column initially had sulfate concentrations typical of seawater. At the high basement fluid discharge rates modeled by Silver et al. (2000) and Fisher et al. (2003a), either model can easily supply enough sulfate to the basal sediments. The precise nature of permeability distribution in the igneous section, required to link lateral fluid flow in the basement with pore fluid gradients in the basal sediments, remains unclear.

Initial results from Legs 170 and 205 highlighted fluid advection along the décollement at Sites 1043/1255 and 1040/1254. Propane, which is a strong indicator of deeply source fluids because of its thermogenic origin (>80°–90°C required) showed strong peaks within the upper fault zone at ~216 mbsf and in the basal part of the décollement zone at ~355 mbsf. **Kastner et al.** (this volume) document that many other pore fluid species show dramatic variation in the regions of fluid advection. The halogens F and Br are strongly enriched above seawater values in the upper fault and décollement zone and throughout the region in between; F/Cl and Br/Cl show the same patterns, indicating that variations are not simply a consequence of brine concentration in the fluids associated with local gas hydrate formation. Ca concentrations are highest in this same region and are associated with highest F concentrations in the pore fluids. Lowest $^{87}Sr/^{86}Sr$ ratios measured at Site 1040/1254 (**Kastner et al.,** this volume, their fig. F4C) and $\delta^{7}Li$ (**Kastner et al.,** this volume, their fig. 6B) values are seen in the upper fault and décollement. Both isotopic tracers show values in those horizons well below anything measured in the incoming sediment section, indicating a fluid source that is not primarily derived from local compacting sediments. Rather, it is advected from a source with high Ca and lower Sr isotopes than appropriate for fluids in equilibrium with marine sediments. Possible sources for this fluid include the dehydration of subducted altered basaltic crust or of the Nicoya ophiolite complex further downdip. Sharp gradients between the underthrust sediment and the décollement zone, seen in K, Li, Ba, F, and Br concentrations and Sr isotopic composition (**Kastner et al.,** this volume) limit the role of fluids derived by local compaction dewatering and vertical advection from below. Any mixing between deeply sourced and local fluids must preserve the very sharp gradients observed.

Haeckel (this volume) modeled the propane profiles in the upper fault zone and in the décollement zone using data from Leg 205 (Morris, Villinger, Klaus, et al., 2003). The two peaks seen at these intervals are asymmetric, with very abrupt bounds at greater depths and more gradual bounds at the shallower depth. This asymmetry requires a vertical advection rate of ~0.4 cm/yr to match. A lateral flow rate cannot be constrained by modeling, as the width of the zone of fluid advection, rate of propane production at depth, and fluid flow rate were combined into a single source term. A constant propane source term of 22 ppm V/yr across a 10-cm-wide conduit could produce the peaks observed, as could lower rates across wider conduits. In the former case, modeling suggests that the upper conduit has been active for ~2000 yr and the lower for ~4000 yr. These results are consistent with suggestions of transient dewatering at other prisms (Bekins et al., 1995; Saffer and Bekins, 1998), albeit on much shorter timescales. As discussed below, long-term

monitoring at Site 1255 includes an experiment for determining fluid flow rates.

Composition of Incoming and Subducting Sediments

Good recovery of the entire incoming sediment column at Site 1039/1253 makes this an excellent reference section for determining the composition of the sediments carried into the subduction zone. Legs 170 and 205 also showed that the entire sediment section of the incoming plate is present beneath the décollement at Sites 1043/1255 and 1040/1254 (see Fig. F3), compacted and dewatered somewhat, but intact and allowing no frontal sediment accretion (Kimura, Silver, Blum, et al., 1997; Morris, Villinger, Klaus, et al., 2003). Building on samples cored from these sites, authors in this volume determine the initial composition of the incoming sediments as well as investigate how the earliest stages of plate subduction, with associated diagenesis and compaction dewatering, may change the composition of the subducting sediments. The correlative changes in pore fluid chemistry are addressed above.

In order to make the comparisons between equivalent horizons on the incoming plate and beneath the décollement, two things are necessary. First is an assumption that sediments at the two sites were of identical composition at the time of deposition (i.e., steady state pertained in sediment deposition and composition over the space and time represented by Sites 1039 and 1040/1254). For comparison, Site 1039 is ~1 km seaward of the deformation front, with Site 1040/1254 being ~1.5 km arcward of the deformation front. At a convergence rate of 88 mm/yr (DeMets et al., 1990) the time difference between the two sites is ~27 k.y. with ~17 k.y. spent in transit beneath the décollement. The second necessity is that the differences in thickness of correlative lithologic units is due only to compaction, justified by previous discussions of lithologic repetition of the lithology outboard of the trench and below the décollement. Estimates of compaction dewatering between Sites 1039 and 1040 were made during Leg 170 and subsequently (Kimura, Silver, Blum, et al., 1997; Saffer et al., 2000). The two estimates are in generally good agreement for Unit U1 (36% compaction) and Subunits U2A (36%), U2B, and U3C (62%). Correlative depths at Site 1040/1254 for the carbonate section Unit 3 are ~15 m deeper using the method of Kimura, Silver, Blum, et al. (1997). In what follows, each set of authors uses their preferred method, meaning that caution should be used in directly comparing the different data sets.

Li and Bebout (this volume, 2005) examine the downhole variations in nitrogen concentrations and isotopes and in carbon abundances and isotopes (in both total organic carbon [TOC] and carbonate) in sediments from both the incoming plate and prism sites to constrain sources for organic matter and paleoproductivity. A first issue to address is possible alteration of original characteristics through diagenesis. Using constraints from the literature and the restricted range of variation in TOC/TN in sediments with large systematic downhole variations in concentration and isotopic composition, the authors evaluate diagenesis as being largely unimportant. Measured C and N isotope compositions imply a dominantly marine source for the organic matter at Site 1039, with mixed marine and terrestrial input of organic matter to the sediments above the décollement.

At Site 1039, TN and TOC increase significantly in the upper 150 m, largely reflecting a change in lithology from carbonate to hemipelagic

sediments. Within the hemipelagics, variations in abundance and isotopic composition are noted and attributed to variation in productivity since the Pliocene. Li and Bebout (2005) speculate that these productivity changes relate to closing of the Central American Seaway, most rapid from 4.6 to 2.6 Ma and completed by ~2 Ma, which resulted in changing ocean circulation and upwelling patterns. The nearer approach of Site 1039 to the trench over time could also bring the site into areas of higher productivity nearer the coastline. These authors calculate that sediment subduction feeds ~1.3 × 10^{10} g/yr N (mean $\delta^{15}N$ = 5.7‰), 1.4 × 10^{11} g/yr TOC (mean $\delta^{13}C$ = –22‰), and 1.5 × 10^{12} g/yr oxidized C (mean $\delta^{13}C$ = 1.9‰) into a section of the MAT ~1100 km long.

N and C isotope systematics of the forearc sediments are reported in **Li and Bebout** (this volume). TN and TOC in the wedge sediments above the décollement are similar to those measured in the hemipelagic section of Site 1039, although the depth-dependent variation is quite different between the two sites. N isotopes from Site 1040 show a more restricted range than at Site 1039 but with similar average values; $\delta^{13}C$ in the TOC is more negative (1‰–2‰) at Site 1040, leading to the identification of a larger proportion of TOC from terrestrial sources. In detail, the downhole variations are different at Site 1040, with maxima in TN, $\delta^{15}N$, and pore fluid ammonium concentrations peaking at ~130–150 mbsf (see **Li and Bebout,** this volume, their fig. F2). These maxima occur below the lithologic boundary between Subunits P1A and P1B. Aside from pore fluid ammonium, no other obvious changes in sediment or pore fluid chemistry occur at this depth (Kimura, Silver, Blum, et al., 1997). Above this depth, the C-N systematics for the wedge sediments at Site 1040 are more similar to those seen farther upslope at Site 1041 than those at Site 1039, again suggesting that the wedge sediments at the very nose of the prism are most likely derived by slumping or debris flows rather than from paleoaccretion (**Li and Bebout,** this volume). Considerable scatter of the data points about the best fit lines for downhole variation in C and N concentrations and isotopes makes it difficult to identify small excursions in the vicinity of the upper faults and the décollement. In the décollement zone, TN, $\delta^{15}N$, and TOC increase slightly, toward values typical of the top of the incoming section. In the top of the décollement zone, TOC $\delta^{13}C$ drops to the most negative values measured in either hole.

Strasser et al. (this volume) also examine stable isotope compositions, measuring $\delta^{13}C$ and $\delta^{18}O$ in bulk carbonate sediments and comparing values between correlative horizons in the incoming sediments at Site 1039/1253 and the underthrust sediments at Site 1040. $\delta^{13}C$ values measured by Strasser et al. are similar to those measured in carbonate by Li and Bebout (2005). The records of downhole variation at Sites 1039 and 1040 generally overlap each other within analytical error (see **Strasser et al.,** this volume, their fig. F5), with several exceptions. Using decompacted depths for Site 1040 that are correlative to Site 1039 depths, the underthrust sediments have higher $\delta^{18}O$ between 228 and 246 mbsf, 288 and 296 mbsf, and 350 and 372 mbsf and lower values between 310 and 330 mbsf. Carbon isotopes for the two cores are different only between 300 and 330 mbsf. The horizons where measurable change in $\delta^{18}O$ occurs between incoming and underthrust sections do not differ appreciably from adjacent intervals in terms of lithology (e.g., weight percent $CaCO_3$) or physical properties but are areas of local maxima in Cl content (Kimura, Silver, Blum, et al., 1997).

As a complement to the study of Ba and sulfate in pore fluids, **Solomon et al.** (this volume) also examine Ba concentrations in bulk samples of correlative sediments at Sites 1039 and 1040 (**Solomon et al.,** this volume, their fig. F5). In Units U2 and U3, values measured for correlative horizons generally scatter around the 1:1 line, indicating similar values in the incoming bulk sediments and their underthrust equivalents. In Unit U1, four samples show Ba concentrations in the underthrust sediments that are much lower than in their correlatives in the incoming section; one sample shows the opposite relationship. Given the pore fluid Ba profiles, one might expect to see maximum departure from the 1:1 line (i.e., greatest Ba loss from the sediment) in the shallowest underthrust sediments, but no simple systematics between Ba loss and depth are observed. The authors speculate that the variability could be due to varying amounts of barite in the different bulk sediment samples; sequential barite extraction and analysis is under way to test this idea.

Implications for Subduction Recycling

The recognition that barite solubility linked to progressive pore water sulfate exhaustion could liberate Ba to the fluid as the sediments subduct is provocative, particularly in combination with the literature on Ba recycling in arcs. Average Ba concentrations in a number of different arcs show good correlation with the subducting Ba flux, as determined from the composition of the incoming sediments outboard of each margin (Plank and Langmuir, 1993, 1998). Studies of prograde metamorphic suites exhumed from the hanging wall of paleosubduction zones typically show marked decreases in the abundance of elements such as B, Cs, and Pb but not Ba with increasing metamorphic grade and volatile loss (Bebout et al., 1999; Morris and Ryan, 2003). Taken together, the metamorphic and arc chemistry studies suggest that Ba mobility at depth is not a significant effect, whereas **Solomon et al.** (this volume) show Ba liberation to a fluid during subduction. Understanding the relative amounts of Ba in barite vs. other less soluble phases in the incoming sediments will be important in resolving this apparent contradiction, along with understanding the partitioning of any liberated Ba between the fluid and other Ba hosts in the sediments such as white micas. The possibility that high F concentrations in subduction zone fluids may help complex and transport trace metals normally regarded as immobile also needs investigation (**Kastner et al.,** this volume).

Plate subduction along ~40,000 km of modern-day convergent margins carries large amounts of volatiles into the deeper Earth. Their devolatilizaton behavior as the plate subducts, their contributions to arc magmatism, and their impact on the deep mantle beyond the arc are largely unconstrained at present. Li and Bebout (2005) compared the sedimentary C and N fluxes into the subduction zone along the MAT with volatile fluxes out of the CAVA to better understand the C and N cycling through subduction zones. Estimates for the N flux out of the arc range from 3.6×10^8 g/yr to 8.2×10^9 g/yr, with C flux estimated at 6.9×10^{11} g/yr (Zimmer et al., 2004; Hilton et al., 2002). As expected, there are large uncertainties in the volcanic flux estimates, and the subducted flux calculated above does not include any N or C bound in alteration phases in the oceanic crust or in any material that may be eroded from the forearc. Even so, the sediment flux into the subduction zone is calculated to be at least 2–5 times greater than the volcanic flux out of it. This gives rise to the question of what happens to the rest of

the subducting C and N. Shaw et al. (2003) report and use data from Site 1039 and the volcanic arc to argue that ~86% of subducted C is carried beyond the arc to the deep mantle. Data from subduction zone and ultra-high-pressure (UHP) metamorphic rocks suggest that N may also subduct to >90 km depth.

Biomarkers at Leg 205 Sites

With the documented flow of methane, propane, and higher hydrocarbons along the upper fault zones and the décollement, the prism sites from Leg 205 in particular are interesting targets for biogeochemical studies. Cardace et al. (this volume) carried out a variety of biomarker analyses on cellular components extracted form lyophilized sediment to identify deoxyribonucleic acid (DNA) and screen for methanogens, quantify eubacterial and Archeal biomass, and evaluate microbial respiratory strategies (aerobic vs. anaerobic). The bulk of samples reported are from Site 1254, cored only around the upper fault zone and décollement region.

The most notable result is that biomarker indicators of microbial activity range from very low to absent. DNA was identified in half of the samples analyzed; methanogen-specific genes were detected in four samples from the sedimentary prism. Working near detection limits for many analyses, it is difficult to pick out meaningful downhole variations at Site 1254 or possible correlations with sediment or pore fluid chemistry or variations in physical properties such as porosity. Highest concentrations of quinones, sometimes treated as a proxy for total biomass (Hiraishi et al., 1998), are associated with the décollement zone in a region where highest Li concentrations suggest most vigorous flow of deeply sourced fluids. Thus, it's likely that viable methanogenic populations exist within the sediment wedge and décollement, but the extremely low temperatures in this region limit their growth.

Physical and Hydraulic Properties across the Margin

The hydraulic and physical properties of the incoming and overlying sediments and décollement zone were important objectives for Legs 170 and 205. Their link to the structural character of the wedge and fluid flow processes were explicitly explored in the Leg 170 *Scientific Results* volume (Silver, Kimura, and Shipley, 2001; Bolton et al., 2000).

Vertical permeabilities of subducted sediments were measured on 14 samples from whole rounds from Legs 170 (Site 1040) and 205 (Sites 1253, 1254, and 1255) by **Screaton et al.** (this volume) and **McKiernan and Saffer** (this volume). The results confirm the low permeabilities of the hemipelagic mud sediments on the order of 10^{-16} to 10^{-20} m^2 with on average slightly higher values up to 10^{-15} m^2 for pelagic carbonate samples. Porosities range between 26% and 71% and show a clear inverse correlation with permeability. **McKiernan and Saffer** (this volume) determined consolidation behavior on samples from Sites 1253, 1254, and 1255 (Leg 205) by constant rate of strain tests.

Screaton and Saffer (2005) use one-dimensional (1-D) and two-dimensional (2-D) fluid flow modeling to explore the impact of rapid loading on fluid expulsion from underthrust sediments as they pass beneath the overlying sediment wedge. In their modeling, they used the measured permeability-porosity relationships and pore pressures inferred from consolidation tests. Their 1-D simulations match observed

values if the estimated permeability of the wedge and décollement is greater than or equal to 5×10^{-17} m^2. Their 2-D models indicate decreasing pore pressure upward in the underthrust hemipelagic sediments and seaward in the carbonate section, which would tend to drive flow vertically toward the décollement in the hemipelagic sediments and laterally toward the deformation front in the carbonate section. The authors note that some of the pore fluid chemical data discussed previously are not consistent with fluid drainage into the décollement and indicate the need for detailed flow, transport, and reaction modeling to resolve the inconsistencies. Screaton and Saffer (2005) note the lower permeabilities of the Costa Rica margin, in contrast to those of Nankai or northern Barbados. In the latter two cases, high décollement permeabilities correspond to modeled and observed fluid flow rates that are too high to be sustained continuously because fluid loss quickly exceeds incoming fluid supply. In Costa Rica, fluid supplies are much greater, in part because of the high convergence rate (~2 times faster than Nankai and nearly 4 times faster than Barbados). Faster rates and complete sediment subduction beneath Costa Rica mean significantly greater fluid flux (24 m^3/yr vs. ~5 m^3/yr at Nankai and Barbados). In combination with lower permeabilities, Costa Rica has the potential to maintain continuous high flow rates along the décollement.

Long-Term Monitoring across the Costa Rica Convergent Margin

Following installation of two CORK-II observatories at Sites 1255 and 1253 during Leg 205 (Morris, Villinger, Klaus, et al., 2003; Jannasch et al., 2003) in October–November 2002, there have been several return visits to collect data and samples. An *Alvin* dive in November 2002 corrected minor problems that had occurred during installation, ensured proper functioning of the pressure monitoring system, and downloaded initial pressure records. A series of *Alvin* dives in March 2004 downloaded pressure data from both sites. Dives had also been planned to recover the OsmoSampler packages and deploy new ones at the two sites. For a variety of reasons (Shipboard Scientific Party, 2004), these efforts failed. During an IODP transit in September 2004, IODP Expedition 301T spent 4 days recovering the originally deployed OsmoSamplers and replacing them with new packages including temperature loggers intended to monitor temperature and collect water samples for 3.5 yr. At Site 1253, OsmoSamplers were lost during recovery but could be located on the seafloor close to Site 1253; the upper sampler was safely returned. Given the timing of the various operations, pressure records run from November 2002 to March 2004, whereas temperature and fluid chemistry data are available from November 2002 to September 2004. Details of the installation (Morris, Villinger, Klaus, et al., 2003) and of methods of long-term fluid sampling and pressure and temperature monitoring are described in Jannasch et al. (2003) and in **Heesemann et al.** (this volume). Interpretation of the first pressure records (Davis and Villinger, 2006) and temperature time series (**Heesemann et al.,** this volume) demonstrate that the installations deliver a wealth of data whose integrated interpretation especially in conjunction with chemical data is still under way.

Objectives for the monitoring are slightly different at the two sites. At Site 1253, the primary goals are to (1) determine temporal variations in pressure and temperature and the state of the igneous basement in

order to constrain the role of the basement as a pathway for fluid flow; (2) determine the origin of the basement fluid (seawater recharge, ridge-flank hydrothermal fluids, or from the deeper subduction zone); and (3) characterize fluid fluxes responsible for the low heat flow at this site. Related to the last are goals of determining solute and gas fluxes to seawater and the residual fluxes to the subduction factory. At the décollement Site 1255, the primary goals are to (1) determine pressure and temperature state of the décollement and the hanging wall of the thrust; (2) determine temporal variation in pressure, temperature, and hydrogeochemical fluxes and their response to tectonic events; and (3) determine the source(s) of fluid in the décollement, again with implications for fluxes to seawater and the deeper subduction zone.

Monitoring on the Incoming Plate at Site 1253

Initial borehole results from Site 1253 are compatible with the scenario discussed earlier, of vigorous flow through permeable horizons in the igneous section, with such flow being recent to contemporary. As shown in Figure **F15,** pressure observations show a relatively rapid decrease in the first 2 months followed by a more gradual decrease throughout the 1.5-yr record. After the initial recovery the upper and lower sensors recorded virtually the same values, indicating that basement is in near-hydrostatic condition despite the proximity to the consolidating subduction complex (Davis and Villinger, 2006). This suggests that it is probably highly permeable and well ventilated to the ocean, consistent with inferences from thermal observations made across the prism and incoming plate (Fisher et al., 2003b; Hutnak et al., 2006) that show the seafloor heat flux to be only a small fraction (as little as 1%) of that expected from the underlying lithosphere. High basement permeability and efficient ventilation at distant basement outcrops are suggested also by geochemical observations made in sediments above the basement contact that show basement water composition to be very similar to seawater (**Kastner et al.,** this volume). Rapid fluid flow within the sediment-buried oceanic crust and efficient advective exchange with the ocean are implied.

Given its ability to maintain a low-pressure state, basement has the capacity to serve as an efficient hydrologic "drain," channelling fluids expelled from the prism and subducted sediments.

The temperature record shows a smooth recovery to a formation fluid temperature of 7.944°C at the end of the end of the recording period (**Heesemann et al.,** this volume). An excursion to lower temperatures occurred when the attempted recovery with the *Alvin* broke the seal and exposed the borehole to the cooler temperatures of bottom seawater. Heat flow at this site derived from the equilibrium downhole temperature is quite low, ~10 ± 0.6 mW/m² (**Heesemann et al.,** this volume) and in good agreement with seafloor measurements (Hutnak et al., in press).

Temporal variations in fluid composition at Site 1253 yield several provocative results (Kastner et al., 2005). Postcruise measurements show that the formation fluid (Fig. **F15**) has steady-state Mg concentrations at approximately half of seawater value; Ca is 3 times seawater value. Sr isotopic compositions measured in the fluid (0.70963) are greater than seawater values, past or present. These compositional features show that the fluid could be derived by mixing local bottom water with altered basement fluids sampled by the TicoFlux cruises; Fisher et al., 2003a) just outboard of Site 1253 or by mixing with fluids derived

F15. P-T variations, p. 52.

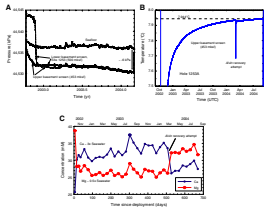

from deeper in the subduction zone (Kastner et al., 2005). In either case, the Sr isotopes suggest that the fluid must also have interacted with sediments containing some older continental component. Such elevated ratios are not measured in pore fluids anywhere in the overlying sediment section at Site 1253. As seen in Figure **F15,** Ca and Mg concentrations show sharp changes following the original sealing of the borehole in November 2002, and again following the *Alvin* recovery attempt, which may be used to calculate flow rates. Fluid velocities are estimated at 45 m/yr immediately following deployment and 7 m/yr following the *Alvin* attempt. It should be noted, however, that additional hydrologic testing and modeling and carbon dating of the formation fluids is necessary before these estimates can be regarded as robust.

The pressure, temperature, and chemical records from Site 1255, shown in Figure **F16,** are quite remarkable. The décollement and overlying prism are observed to be superhydrostatic during the monitoring period (Fig. **F16**) but only moderately so. Even the maximum pressure observed early in the observation period, 250 kPa above hydrostatic, was only ~25% of a lithostatic level. Long-term transient decays are observed at both monitoring levels in Hole 1255A. The origin of the initially elevated pressures can only be speculated about. The last major thrust earthquake that occurred in this region in 1950 is an unlikely candidate; some other more recent deformational event, either aseismic (like those witnessed by Protti et al., 2004), or with associated seismicity (as in the case of a nearby Mw = 6.4 earthquake in July 2000), could be responsible. Except at the base of the sediments (which must remain at a near-hydrostatic state for some distance landward of the prism toe), no constraints are provided about levels of overpressure in the underthrust section, where greater overpressures are expected (given their greater hydrologic isolation) and inferred (on the basis of consolidation test results). Targeting the underthrust sediment section for monitoring was precluded during Leg 205 because of the difficulty and time needed to install instrumentation with the technology employed. Consolidation tests (Saffer, 2003; Saffer et al., 2000) suggest the presence of relatively high pressures, but they provide only indirect estimates and provide no information about temporal variations.

Formation temperatures at Site 1255 are 3.58°C at the base of the overthrust prism sediment section and 3.64°C at a level 5 m deeper within the décollement, resulting in a heat flow of ~11 mW/m². Temperature equilibrates at Site 1255 more rapidly than at Site 1253; this could reflect differences in the CORK configurations at the two sites or could be due to a much greater and longer inflow of cold seawater during drilling at Site 1253. In contrast, drilling operations at Site 1255 were much shorter, permeability is much lower, and the formation pressures are superhydrostatic. Unfortunately, the last submersible visit to download pressure data occurred during early March 2004; therefore, no pressure data currently exist for the end of the fluid sampling and temperature records.

Two small stepwise pressure offsets superimposed on the generally smooth decay in pressure occurred during the observation period at Site 1255 in the upper and lower screens (Fig. **F16**). The first event occurred in late May to early June 2003 and is manifested by a sharp increase in pressure within the décollement of ~30 kPa and a smaller pressure transient in the overlying sediments of opposite polarity. After the first event, the long-term transient decline in pressure in the décollement disappeared and temperatures remained elevated for 2 months. The second event occurred during mid-September to late October 2003. De-

F16. Pressure variations, p. 53.

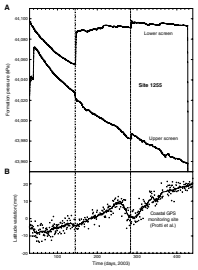

tailed aspects of these (including inconsistent signs and offsets in timing; an end of decreasing pressure at the décollement at the time of the first step; correlative temperature and geochemical transients) do not lead to any obvious explanation regarding their origin, although a clear association between these pressure steps and two deformational events was observed during a GPS strain monitoring experiment (see Fig. F16) that was under way on the Nicoya Peninsula, directly onshore from the borehole sites, during much of the CORK monitoring epoch described here. Similar correlations, albeit at different times, are observed between diffuse fluid flow and seismic activity in this region (Brown et al., 2005). In both cases, the prism pressure offsets (24 May and 12 October 2003) occurred 2–3 weeks after the initiation of the onshore strain events (Fig. F16). If their origin is local strain, not hydrologically transmitted pressure, the magnitude of volumetric strain suggested would be somewhat greater than 10^{-6} (Davis and Villinger, 2006).

The chemical results at Site 1255 are also tantalizing. Figure F17 uses temporal variation in NH_4 concentrations to show that the events affecting pressure and temperature in June and October 2003 also affect the chemistry of the fluids. The decreasing NH_4 during Event 1 is accompanied by increasing Cl at values above seawater, indicating Event 1 is not simply leaking of seawater through the packer seal (Kastner et al., 2005). The changes in fluid composition indicate that these events are not just changes in hydraulic properties of the wedge in the vicinity of the samplers but must include changes in the fluid sources or in mixing proportions between sources. As shown, Event 1 could include a greater admixture of fluids with NH_4 contents similar to those squeezed from the underthrust sediments, and Event 2 incorporates a greater proportion of fluids derived either from prism sediments above the décollement or advected from farther downdip. Strikingly, salinity contents for formation fluids are above seawater values and increase through time (Kastner et al., 2005), which they attribute to in situ gas hydrate formation. Preliminary results from these same authors suggest that the flow meter experiment deployed at this site (Jannasch et al., 2003) worked well and that Events 1 and 2 are associated with significant changes in relative fluid flow rates.

F17. Ammonium concentrations, p. 54.

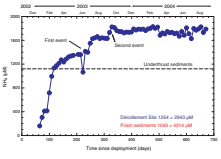

CONCLUSIONS

ODP Legs 170 and 205 helped define and address objectives for subduction factory and seismogenic zone studies in Central America. Between the active monitoring of fluid flow across the Middle America Trench in Costa Rica and the postcruise science of sedimentary and igneous samples the legs provide the basis for an integrated study of the margin. This includes the sedimentary and igneous character of the incoming plate, its thermal structure, and evidence for multiple episodes of fluid flow, including recent to contemporary flow in a cold setting far off-axis. It also includes the structure, sedimentology, geochemistry, and permeability characteristics of the forearc sediment wedge, décollement, and underthrust sediments. Interesting in their own right, these studies also provide context for the monitoring of active flow of deeply sourced fluids along the décollement and the link between fluid flow and the seismic cycle.

Studies of the incoming plate speak to modification of the crust generated at the East Pacific Rise and to multiple episodes of fluid flow.

Coring, petrology, and geochemistry show extensive addition (>180 m) of enriched basaltic material, with characteristics of ocean island basalt, to the upper part of the incoming igneous section. The sills and intrusions cored during Leg 170 and 205 form part of a large region of off-axis magmatism, with ages of ~14 and perhaps 8–10 Ma; seamounts and Cocos track tholeiites have similar chemical characteristics to those reported here. Speculation is that fractures and stresses associated with plate rearrangement allowed distal emplacement of enriched mantle (from the Galapagos hotspot?) into the depleted upper mantle, with later tectonic events or magmatic heating triggering melting. Although the rocks are little altered overall, Sr isotope studies reveal localized intervals (<10–20 m thick) of major isotopic shifts (from ~0.7033 to 0.705), requiring water:rock ratios >6. Two fluids, one of which is significantly altered from seawater composition, best satisfy modeling. One alteration horizon is monitored by our downhole instruments, where results to date indicate a vigorous regime of active flow in permeable layers that are slightly subhydrostatic. Chemical data from the collected fluids imply mixing between bottom seawater and a second fluid, which is greatly enriched in Ca and depleted in Mg relative to seawater. Fluid flow rates estimated from various methods (heat flow, pore fluid gradients in overlying sediments, and recovery of formation fluids from seawater composition after closing the borehole) are all on the order of meters per year. Ash deposits on the incoming plate record siliceous explosive volcanic activity in the CAVA over the last 2.5 m.y. Based on various chemical tracers, arc lavas recorded a peak in subducted input (fluids and sediments) at ~1.45 Ma, with lesser contributions before and since.

Studies from the prism sites focus on the origin of the sediments above the décollement, the permeability structure, and biogeochemistry. Sediments from Leg 205 cored just above the décollement are early Pliocene in age, but no younger than 3.75 Ma, as are those between 219 and 222 mbsf. Prism sediments between 150 and 161 mbsf are of early Pleistocene age, and those between 161 and 216 mbsf are late Pliocene. Sediments from Subunit P1B have C and N systematics more like those measured upslope at Site 1041 than the incoming sediment section, consistent with Leg 205 shipboard analyses suggesting that the prism sediments are derived from slumping rather than paleoaccretion. Biomarker indicators of microbial activity range from very low to absent. DNA was identified in half of the samples analyzed; methanogen-specific genes were detected in four samples from the sedimentary prism. Highest concentrations of quinones, sometimes treated as a proxy for total biomass (Hiraishi et al., 1998), are associated with the décollement zone. Measurements of permeability and porosity confirm the low permeabilities of the hemipelagic mud sediments on the order of 10^{-16} to 10^{-20} m^2 with on average slightly higher value of up to 10^{-15} m^2 for pelagic carbonate samples. Porosities range between 26% and 71% and show a clear inverse correlation with permeability. Long-term monitoring in the décollement zone at Site 1255 shows that flow in the prism sediments and décollement is slightly superhydrostatic. Excursions in the pressure record are observed in late May–early June 2003 and in mid-September to late October 2003; these occur 2–3 weeks after deformational events recorded geodetically. Chemical excursions and changes in flow rate are also associated with these events.

ACKNOWLEDGMENTS

We want to express our deep gratitude to many. Many of the original goals for Leg 205 were defined or refined as a result of Leg 170, and we thank Leg 170 Co-Chief Scientists Eli Silver and Gaku Kimura, Staff Scientist Peter Blum, and their entire shipboard science party. Regretfully, Marcus Langseth was not able to be part of that team, but his role in identifying the anomalous heat flow in the region, and its causes, was central to Leg 205. The Leg 205 shipboard science party has been great. They worked intensely while core was coming up, did important intellectual work during the lulls for downhole engineering, and have carried out high-quality postcruise science; our special thanks to you all. Adam Klaus has been a tremendous asset as Staff Scientist. Shore-based participants have been an essential part of Leg 205 monitoring and science. In addition to those represented in this volume, we express our grateful appreciation for the work done by Earl Davis, Hans Jannasch, Geoff Wheat, and their collaborators. The observatory installations required all the determination, innovation, and know-how of Tom Pettigrew and the entire drilling and operations crew for Leg 205, and to you we extended our deepest appreciation. This manuscript was greatly improved by helpful and constructive comments from P. Castillo, A. Fisher, and E. Silver. This research used samples and/or data provided by the Ocean Drilling Program (ODP). ODP is sponsored by the U.S. National Science Foundation (NSF) and participating countries under management of Joint Oceanographic Institutions (JOI), Inc.

REFERENCES

Albarède, F., 2003. *Geochemistry:* Cambridge (Cambridge Univ. Press).

Abratis, M., and Woerner, G., 2001. Ridge collision, slab-window formation, and the flux of Pacific asthenosphere into the Caribbean realm. *Geology,* 29(2):127–130. **doi:10.1130/0091-7613(2001)029<0127:RCSWFA>2.0.CO;2**

Barckhausen, U., Ranero, C.R., von Huene, R., Cande, S.C., and Roeser, H.A., 2001. Revised tectonic boundaries in the Cocos plate off Costa Rica: implications for the segmentation of the convergent margin and for plate tectonic models. *J. Geophys. Res.,* 106(B9):19207–19220. **doi:10.1029/2001JB000238**

Barckhausen, U., Roeser, H.A., and von Huene, R., 1998. Magnetic signature of upper plate structures and subducting seamounts at the convergent margin off Costa Rica. *J. Geophys. Res.,* 103(B4):7079–7094. **doi:10.1029/98JB00163**

Bebout, G.E., Ryan, J.G., Leeman, W.P., and Bebout, A.E., 1999. Fractionation of trace elements by subduction-zone metamorphism-effect of convergent-margin thermal evolution. *Earth Planet. Sci. Lett.,* 171(1):63–81. **doi:10.1016/S0012-821X(99)00135-1**

Becker, K., Fisher, A.T., and Davis, E.E., 1997. The CORK experiment in Hole 949C: long-term observations of pressure and temperature in the Barbados accretionary prism. *In* Shipley, T.H., Ogawa, Y., Blum, P., and Bahr, J.M. (Eds.), *Proc. ODP, Sci. Results,* 156: College Station, TX (Ocean Drilling Program), 247–252. [**PDF**]

Becker, K., the Leg 174B Scientific Party, and Davis, E.E., 1998. Leg 174B revisits Hole 395A: logging and long-term monitoring of off-axis hydrothermal processes in young oceanic crust. *JOIDES J.,* 24:1–3, 13.

Bekins, B.A., McCaffrey, A.M., and Driess, S.J., 1995. Episodic and constant flow models for the origin of low-chloride waters in a modern accretionary complex. *Water Resour. Res.,* 31(12):3205–3216. **doi:10.1029/95WR02569**

Berggren, W.A., Kent, D.V., Swisher, C.C., III, and Aubry, M.-P., 1995. A revised Cenozoic geochronology and chronostratigraphy. *In* Berggren, W.A., Kent, D.V., Aubry, M.-P., and Hardenbol, J. (Eds.), *Geochronology, Time Scales and Global Stratigraphic Correlation*. Spec. Publ.—SEPM (Soc. Sediment. Geol.), 54:129–212.

Bolton, A.J., Vannucchi, P., Clennell, M.B., and Maltman, A., 2001. Microstructural and geomechanical constraints on fluid flow at the Costa Rica convergent margin, Ocean Drilling Program Leg 170. *In* Silver, E.A., Kimura, G., Blum, P., and Shipley, T.H. (Eds.), *Proc. ODP, Sci. Results,* 170, 1–32 [CD-ROM]. Available from: Ocean Drilling Program, Texas A&M University, College Station TX 77845-9547, USA. [**HTML**]

Brown, K.M., Tryon, M.D., DeShon, H.R., Dorman, L.M., and Schwartz, S.Y., 2005. Correlated transient fluid pulsing and seismic tremor in the Costa Rica subduction zone. *Earth Planet. Sci. Lett.,* 238(1–2):189–203. **doi:10.1016/j.epsl.2005.06.055**

Brumsack, H.-J., and Gieskes, J.M., 1983. Interstitial water trace-metal chemistry of laminated sediments from the Gulf of California, Mexico. *Mar. Chem.,* 14(1):89–106. **doi:10.1016/0304-4203(83)90072-5**

Carr, M.J., Feigenson, M.D., and Bennett, E.A., 1990. Incompatible element and isotopic evidence for tectonic control of source mixing and melt extraction along the Central American arc. *Contrib. Mineral. Petrol.,* 105:369–380.

Carr, M.J., Feigenson, M.D., Patino, L.C., and Walker, J.A., 2003. Volcanism and geochemistry in Central America: progress and problems. *In* Eiler, J. (Ed.), *Inside the Subduction Factory.* Geophys. Monogr., 138.

Chan, L.-H., Leeman, W.P., and You, C.-F., 1999. Lithium isotopic composition of Central American volcanic arc lavas: implications for modification of subarc mantle by slab-derived fluids. *Chem. Geol.,* 160(4):255–280. **doi:10.1016/S0009-2541(99)00101-1**

Chan, L.-H., Leeman, W.P., and You, C.-F., 2002. Lithium isotopic composition of Central American volcanic arc lavas: implications for modification of subarc man-

tle by slab-derived fluids: correction. *Chem. Geol.,* 182(2–4):293–300. **doi:10.1016/S0009-2541(01)00298-4**

Chan, L.-H., and Kastner, M., 2000. Lithium isotopic compositions of pore fluids and sediments in the Costa Rica subduction zone: implications for fluid processes and sediment contribution to the arc volcanoes. *Earth Planet. Sci. Lett.,* 183(1–2):275–290. **doi:10.1016/S0012-821X(00)00275-2**

Christeson, G.L., McIntosh, K.D., and Shipley, T.H., 2000. Seismic attenuation in the Costa Rica margin wedge: amplitude modeling of ocean bottom hydrophone data. *Earth Planet. Sci. Lett.,* 179(2):391–405. **doi:10.1016/S0012-821X(00)00118-7**

Christeson, G.L., McIntosh, K.D., Shipley, T.H., Flueh, E., and Goedde, H., 1999. Structure of the Costa Rica convergent margin, offshore Nicoya peninsula. *J. Geophys. Res.,* 104(B11):25443–25468. **doi:10.1029/1999JB900251**

Clift, P., and Vannucchi, P., 2004. Controls on tectonic accretion versus erosion in subduction zones: implications for the origin and recycling of the continental crust. *Rev. Geophys.,* 42(2):RG2001. **doi:10.1029/2003RG000127**

Clift, P.D., Chan, L-H., Blusztajn, J., Layne, G.D., Kastner, M., and Kelly, R.K., 2005. Pulsed subduction accretion and tectonic erosion reconstructed since 2.5 Ma, from the tephra record offshore Costa Rica. *Geochem., Geophys., Geosyst.,* 6(9):Q09016. **doi:10.1029/2005GC000963**

Davis, E.E., and Villinger, H.W., 2006. Transient formation fluid pressures and temperatures in the Costa Rica forearc prism and subducting oceanic basement: CORK monitoring at ODP Sites 1253 and 1255. *Earth Planet. Sci. Lett.,* 245(1–2):232–244. **doi:10.1016/j.epsl.2006.02.042**

Davis, E.E., Wang, K., Becker, K., and Thomson, R.E., 2000. Formation-scale hydraulic and mechanical properties of oceanic crust inferred from pore pressure response to periodic seafloor loading. *J. Geophys. Res.,* 105(B6):13423–13436. **doi:10.1029/2000JB900084**

DeMets, C., Gordon, R.G., Argus, D.F., and Stein, S., 1990. Current plate motions. *Geophys. J. Int.,* 101:425–478.

Dickens, G.R., 2001. Sulfate profiles and barium fronts in sediment on the Blake Ridge: present and past methane fluxes through a large gas hydrate reservoir. *Geochim. Cosmochim. Acta,* 65(4):529–543. **doi:10.1016/S0016-7037(00)00556-1**

Dreyer, B., Chavagnac, V., and Morris, J., 2005. Low temperature fluid flow in the permeable igneous complex of the subducting Cocos plate, offshore Costa Rica. *Eos, Trans. Am. Geophys. Union,* 86(52)(Suppl.):T33A-0515. (Abstract)

Dymond, J., Suess, E., and Lyle, M., 1992. Barium in deep-sea sediment: a geochemical proxy for paleoproductivity. *Paleoceanography,* 7:163–181.

Dymond, J., and Collier, R., 1996. Particulate barium fluxes and their relationships to biological productivity. *Deep Sea Res., Part II,* 43:1283–1308. **doi:10.1016/0967-0645(96)00011-2**

Fisher, A.T., 1998. Permeability within basaltic oceanic crust. *Rev. Geophys.,* 36(2):143–182. **doi:10.1029/97RG02916**

Fisher, A.T., Davis, E.E., Hutnak, M., Spiess, V., Zühlsdorff, L., Cherkaoui, A., Christiansen, L., Edwards, K., Macdonald, R., Villinger, H., Mottl, M.J., Wheat, C.G., and Becker, K., 2003. Hydrothermal recharge and discharge across 50 km guided by seamounts on a young ridge flank. *Nature (London, U. K.),* 421:618–621. **doi:10.1038/nature01352**

Fisher, A.T., Stein, C.A., Harris, R.N., Wang, K., Silver, E.A., Pfender, M., Hutnak, M., Cherkaoui, A., Bodzin, R., and Villinger, H., 2003. Abrupt thermal transition reveals hydrothermal boundary and role of seamounts within the Cocos plate. *Geophys. Res. Lett.,* 30(11):1550–1553. **doi:10.1029/2002GL016766**

German, C.R., Bourles, D.L., Brown, E.T., Hergt, J., Colley, S., Higgs, N.C., Ludford, E.M., Nelsen, T.A., Feely, R.A., Raisbeck, G., and Yiou, F., 1997. Hydrothermal scavenging on the Juan de Fuca Ridge: $^{230}Th_{xs}$, ^{10}Be, and REEs in ridge-flank sediments. *Geochim. Cosmochim. Acta,* 61(19):4067–4078. **doi:10.1016/S0016-7037(97)00230-5**

German, C.R., Hergt, J., Palmer, M.R., and Edmond, J.M., 1999. Geochemistry of a hydrothermal sediment core from the OBS vent-field, 21°N East Pacific Rise. *Chem. Geol.,* 155(1–2):65–75. **doi:10.1016/S0009-2541(98)00141-7**

Hacker, B.R., Peacock, S.M., Abers, G.A., and Holloway, S.D., 2003. Subduction factory, 2. Are intermediate-depth earthquakes in subducting slabs linked to metamorphic dehydratation reactions? *J. Geophys. Res.,* 108(B1):2030. **doi:10.1029/2001JB001129**

Harpp, K.S., and White, W.M., 2001. Tracing a mantle plume: isotopic and trace element variations of Galápagos seamounts. *Geochem., Geophys., Geosyst.,* 2(6). **doi:10.1029/2000GC000137**

Hauff, F., Hoernle, K., and Schmidt, A., 2003. Sr-Nd-Pb composition of Mesozoic Pacific oceanic crust (Site 1149 and 801, ODP Leg 185): implications for alteration of ocean crust and the input into the Izu-Bonin-Mariana subduction system. *Geochem., Geophys., Geosyst.,* 4(8):8913. **doi:10.1029/2002GC000421**

Hey, R., 1977. Tectonic evolution of the Cocos-Nazca spreading center. *Geol. Soc. Am. Bull.,* 88(10):1404–1420. **doi:10.1130/0016-7606(1977)88<1404:TEOTCS>2.0.CO;2**

Hilton, D.R., Fischer, T.P., and Marty, B., 2002. Noble gases and volatile recycling at subduction zones. *In* Porcelli, D., Wieler, R., and Ballentine, C. (Eds.), *Noble Gases in Geochemistry and Cosmochemistry.* Rev. Mineral. Geochem., 47:319–370.

Hiraishi, A., Ueda, Y., and Ishihara, J., 1998. Quinone profiling of bacterial communities in natural and synthetic sewage activated sludge for enhanced phosphate removal. *Appl. Environ. Microbiol.,* 64(3):992–998.

Hutnak, M., Fisher, A.T., Stein, C.A., Harris, R., Wang, K., Silver, E., Spinelli, G., Pfender, M., Villinger, H., Pisani, P.C., Deshon, H., and MacKnight, B., in press. The thermal state of 18–24 Ma upper lithosphere subducting below the Nicoya Peninsula, northern Costa Rica margin. *In* Dixon, T., and Moore, J.C. (Eds.), *Seismogenic Zone Earthquakes on the Subduction Thrust:* New York (Columbia Univ. Press).

Ibaraki, M., 2001. Pliocene–Pleistocene paleoceanography in the East Pacific off Costa Rica determined by planktonic foraminifers. *In* Silver, E.A., Kimura, G., Blum, P., and Shipley, T.H. (Eds.), *Proc. ODP, Sci. Results,* 170, 1–28 [CD-ROM]. Available from: Ocean Drilling Program, Texas A&M University, College Station TX 77845-9547, USA. [**HTML**]

Jannasch, H., Davis, E., Kastner, M., Morris, J., Pettigrew, T., Plant, J.N., Solomon, E., Villinger, H., and Wheat, C.G., 2003. CORK-II: long-term monitoring of fluid chemistry, fluxes, and hydrology in instrumented boreholes at the Costa Rica subduction zone. *In* Morris, J.D., Villinger, H.W., Klaus, A., *Proc. ODP, Init. Repts.,* 205: College Station, TX (Ocean Drilling Program), 1–36. **doi:10.2973/odp.proc.ir.205.102.2003**

John, C.M., Mutti, M., and Adatte, T., 2003. Mixed carbonate-siliciclastic record on the North African margin (Malta)—coupling of weathering processes and mid-Miocene climate. *Geol. Soc. Am. Bull.,* 115(2):217–229. **doi:10.1130/0016-7606(2003)115<0217:MCSROT>2.0.CO;2**

Kastner, M., Morris, J., Chan, L.H., Saether, O., and Luckge, A., 2000. Three distinct fluid systems at the Costa Rica subduction zone: chemistry, hydrology, and fluxes. *Goldschmidt 2000, J. Conf. Abstr.,* 5:572. (Abstract)

Kastner, M., Solomon, E., Wheat, G., Jannasch, H., Davis, E., Villinger, H., Heesemann, M., Robertson, G., and Morris, J., 2005. Continuous chemical and fluid flux monitoring in two distinct fluid flow systems at the Costa Rica subduction zone. *Eos, Trans. Am. Geophys. Union,* 86(52)(Suppl.):T12B-02. (Abstract)

Kelly, R.K., 2003. Subduction dynamics at the Middle America Trench: new constraints from swath bathymetry, multi-channel seismc data and ^{10}Be [Ph.D. thesis]. Massachusetts Inst. of Technology, Woods Hole.

Kelly, R.K., and Driscoll, N.W., 1998. Structural controls on ^{10}Be occurrences in arc lavas. *Eos, Trans. Am. Geophys. Union,* 79:45.

Kimura, G., Silver, E.A., Blum, P., et al., 1997. *Proc. ODP, Init. Repts.,* 170: College Station, TX (Ocean Drilling Program). [**HTML**]

Kopf, A., Deyhle, A., and Zuleger, E., 2000. Evidence for deep fluid circulation and gas hydrate dissociation using boron and boron isotopes of pore fluids in forearc sediments from Costa Rica (ODP Leg 170). *Mar. Geol.,* 167(1–2):1–28. **doi:10.1016/S0025-3227(00)00026-8**

Kyte, F.T., Leinen, M., Heath, G.R., and Zhou, L., 1993. Cenozoic sedimentation history of the central North Pacific: inferences from the elemental geochemistry of Core LL44-GPC3. *Geochim. Cosmochim. Acta,* 57(8):1719–1740. **doi:10.1016/0016-7037(93)90109-A**

Langseth, M.G., and Silver, E.A., 1996. The Nicoya convergent margin: a region of exceptionally low heat flow. *Geophys. Res. Lett.,* 23:891–894.

Li, L., and Bebout, G.E., 2005. Carbon and nitrogen geochemistry of sediments in the Central American convergent margin: insights regarding subduction input fluxes, diagenesis, and paleoproductivity. *J. Geophys. Res.,* 110:B11202. **doi:10.1029/2004JB003276**

Lonsdale, P., and Klitgord, K.D., 1978. Structure and tectonic history of the eastern Panama Basin. *Geol. Soc. Am. Bull.,* 89(7):981–999. **doi:10.1130/0016-7606(1978)89<981:SATHOT>2.0.CO;2**

Martini, E., 1971. Standard Tertiary and Quaternary calcareous nannoplankton zonation. *In* Farinacci, A. (Ed.), *Proc. 2nd Int. Conf. Planktonic Microfossils Roma:* Rome (Ed. Tecnosci.), 2:739–785.

McIntosh, K.D., and Sen, M.K., 2000. Geophysical evidence for dewatering and deformation processes in the ODP Leg 170 area offshore Costa Rica. *Earth Planet. Sci. Lett.,* 178(1–2):125–138. **doi:10.1016/S0012-821X(00)00069-8**

McIntosh, K.D., Silver, E.A., and Shipley, T., 1993. Evidence and mechanisms for forearc extension at the accretionary Costa Rica convergent margin. *Tectonics,* 12:1380–1392.

McManus, J., Berelson, W.M., Klinkhammer, G.P., Johnson, K.S., Coale, K.H., Anderson, R.F., Kumar, N., Burdige, D.J., Hammond, D.E., Brumsack, H.-J., McCorkle, D.C., and Rushdi, A., 1998. Geochemistry of barium in marine sediments: implications for its use as a paleoproxy. *Geochim. Cosmochim. Acta,* 62(21–22):3453–3473. **doi:10.1016/S0016-7037(98)00248-8**

Meschede, M., Zweigel, P., and Kiefer, E., 1999. Subsidence and extension at a convergent plate margin: evidence for subduction erosion off Costa Rica. *Terra Nova,* 11(2–3):112–117. **doi:10.1046/j.1365-3121.1999.00234.x**

Moritz, E., Bornholdt, S., Westphal, H., and Meschede, M., 2000. Neural network interpretation of LWD data (ODP Leg 170) confirms complete sediment subduction at the Costa Rica convergent margin. *Earth Planet. Sci. Lett.,* 174(3–4):301–312. **doi:10.1016/S0012-821X(99)00270-8**

Morris, J., Valentine, R., and Harrison, T., 2002. ^{10}Be imaging of sediment accretion, subduction along the northeast Japan and Costa Rica convergent margins. *Geology,* 30(1):59–62. **doi:10.1130/0091-7613(2002)030<0059:BIOSAA>2.0.CO;2**

Morris, J.D., Leeman, W.P., and Tera, F., 1990. The subducted component in island arc lavas: constraints from Be isotopes and B-Be systematics. *Nature (London, U. K.),* 344:31–36.

Morris, J.D., and Ryan, J.G., 2003. Subduction zone processes and implications for changing composition of the upper and lower mantle. *In* Holland, H.D., and Turekian, K.K. (Eds.), *The Mantle and Core* (Vol. 2): *Treatise on Geochemistry:* New York (Elsevier), 451–471.

Morris, J.D., Villinger, H.W., Klaus, A., et al., 2003. *Proc. ODP, Init. Repts.,* 205: College Station, TX (Ocean Drilling Program). **doi:10.2973/odp.proc.ir.205.2003**

Muza, J.P., 2001. Calcareous nannofossil biostratigraphy from a 15-km transect (Cocos plate to Caribbean plate) across the Middle America Trench, Nicoya Peninsula, Costa Rica. *In* Silver, E.A., Kimura, G., Blum, P., and Shipley, T.H. (Eds.), *Proc. ODP, Sci. Results,* 170, 1–63 [CD-ROM]. Available from: Ocean Drilling Program, Texas A&M University, College Station TX 77845-9547, USA. [**HTML**]

Newman, A.V., Schwartz, S.Y., Gonzalez, V., DeShon, H.R., Protti, J.M., and Dorman, L.M., 2002. Along-strike variability in the seismogenic zone below Nicoya Peninsula, Costa Rica. *Geophys. Res. Lett.,* 29. **doi:10.1029/2002GL015409**

Patino, L.C., Carr, M.J., and Feigenson, M.D., 2000. Local and regional variations in Central American arc lavas controlled by variations in subducted sediment input. *Contrib. Mineral. Petrol.,* 138(3):265–283. **doi:10.1007/s004100050562**

Pfender, M., and Villinger, H., 2002. Miniaturized data loggers for deep sea sediment temperature gradient measurements. *Mar. Geol.,* 186(3–4):557–570. **doi:10.1016/S0025-3227(02)00213-X**

Plank, T., and Langmuir, C.H., 1993. Tracing trace elements from sediment input to volcanic output at subduction zones. *Nature (London, U. K.),* 362(6422):739–743. **doi:10.1038/362739a0**

Plank, T., and Langmuir, C.H., 1998. The chemical composition of subducting sediment and its consequences for the crust and mantle. *Chem. Geol.,* 145(3–4):325–394. **doi:10.1016/S0009-2541(97)00150-2**

Protti, M., Gonzalez, V., Kato, T., Iinuma, T., Miyazaki, S., Obana, K., Kaneda, Y., La Femina, P., Dixon, T., and Schwartz, S., 2004. A creep event on the shallow interface of the Nicoya Peninsula, Costa Rica seismogenic zone. *Eos, Trans. Am. Geophys. Union,* 85(47)(Suppl.):F1378. (Abstract)

Protti, M., Guendel, F., and McNally, K., 1994. The geometry of the Wadati-Benioff zone under southern Central America and its tectonic significance: results from a high-resolution local seismographic network. *Phys. Earth Planet. Inter.,* 84(1–4):271–287. **doi:10.1016/0031-9201(94)90046-9**

Ranero, C.R., and von Huene, R., 2000. Subduction erosion along the Middle America convergent margin. *Nature (London, U. K.),* 404(6779):748–752. **doi:10.1038/35008046**

Ranero, C.R., von Huene, R., Flueh, E., Duarte, M., Baca, D., and McIntosh, K., 2000a. A cross section of the convergent Pacific margin of Nicaragua. *Tectonics,* 19(2):335–357. **doi:10.1029/1999TC900045**

Ranero, C.R., von Huene, R., Weinrebe, W., McIntosh, K.D., and Reichert, C., 2000b. Mass transfer and fluid flow paths related to subduction erosion at the Middle America convergent margin. *Eos, Trans. Am. Geophys. Union,* 81(48)(Suppl):T12D-08. (Abstract)

Reagan, M.K., Morris, J.D., Herrstrom, E.A., and Murrell, M.T., 1994. Uranium series and beryllium isotopic evidence for an extended history of subduction modification of the mantle below Nicaragua. *Geochim. Cosmochim. Acta.,* 58(19):4199–4212. **doi:10.1016/0016-7037(94)90273-9**

Ruppel, C., and Kinoshita, M., 2000. Fluid, methane, and energy flux in an active margin gas hydrate province, offshore Costa Rica. *Earth Planet. Sci. Lett.,* 179(1):153–165. **doi:10.1016/S0012-821X(00)00096-0**

Saffer, D.M., 2003. Pore pressure development and progressive dewatering in underthrust sediments at the Costa Rican subduction margin: comparison with northern Barbados and Nankai. *J. Geophys. Res.,* 108(B5):2261–2276. **doi:10.1029/2002JB001787**

Saffer, D.M., and Bekins, B.A., 1998. Episodic fluid flow in the Nankai accretionary complex: timescale, geochemistry, flow rates, and fluid budget. *J. Geophys. Res.,* 103(B12):30351–30371. **doi:10.1029/98JB01983**

Saffer, D.M., Silver, E.A., Fisher, A.T., Tobin, H., and Moran, K., 2000. Inferred pore pressures at the Costa Rica subduction zone: implications for dewatering processes. *Earth Planet. Sci. Lett.,* 177(3–4):193–207. **doi:10.1016/S0012-821X(00)00048-0**

Screaton, E.J., and Saffer, D.M., 2005. Fluid expulsion and overpressure development during initial subduction at the Costa Rica convergent margin. *Earth Planet. Sci. Lett.,* 233(3–4):361–374. **doi:10.1016/j.epsl.2005.02.017**

Shaw, A.M., Hilton, D.R., Fischer, T.P., Walker, J.A., and Alvarado, G.E., 2003. Contrasting He–C relationships in Nicaragua and Costa Rica: insights into C cycling

through subduction zones. *Earth Planet. Sci. Lett.,* 214(3–4):499–513. **doi:10.1016/S0012-821X(03)00401-1**

Shipboard Scientific Party, 2003. Leg 205 summary. *In* Morris, J.D., Villinger, H.W., Klaus, A., *Proc. ODP, Init. Repts.,* 205: College Station, TX (Ocean Drilling Program), 1–75. **doi:10.2973/odp.proc.ir.205.101.2003**

Shipboard Scientific Party, 2004. Costa Rica hydrogeology. *IODP Prel. Rept.,* 301T. **doi:10.2204/iodp.pr.301T.2004**

Shipley, T.H., McIntosh, K.D., Silver, E.A., and Stoffa, P.L., 1992. Three-dimensional seismic imaging of the Costa Rica accretionary prism: structural diversity in a small volume of the lower slope. *J. Geophys. Res.,* 97:4439–4459.

Silver, E., Costa Pisani, P., Hutnak, M., Fisher, A., DeShon, H., and Taylor, B., 2004. An 8–10 Ma tectonic event on the Cocos plate offshore Costa Rica: result of Cocos Ridge collision? *Geophys. Res. Lett.,* 31(18). **doi:10.1029/2004GL020272**

Silver, E., Kastner, M., Fisher, A., Morris, J., McIntosh, K., and Saffer, D., 2000. Fluid flow paths in the Middle America Trench and Costa Rica margin. *Geology,* 28(8):679–682. **doi:10.1130/0091-7613(2000)028<0679:FFPITM>2.3.CO;2**

Silver, E.A., Kimura, G., and Shipley, T.H. (Eds.), 2001. *Proc. ODP, Sci. Results,* 170 [CD-ROM]. Available from: Ocean Drilling Program, Texas A&M University, College Station TX 77845-9547, USA. [**HTML**]

Spinelli, G.A., and Saffer, D.M., 2004. Along-strike variations in underthrust sediment dewatering on the Nicoya margin, Costa Rica related to the updip limit of seismicity. *Geophys. Res. Lett.,* 31(4):L04613. **doi:10.1029/2003GL018863**

Stein, C.A., and Stein, S., 1992. A model for the global variation in oceanic depth and heat flow with lithospheric age. *Nature (London, U. K.),* 359(6391):123–129. **doi:10.1038/359123a0**

Tobin, H., Vannuchi, P., and Meschede, M., 2001. Structure, inferred mechanical properties, and implications for fluid transport in the décollement zone, Costa Rica convergent margin. *Geology,* 29(10):907–910. **doi:10.1130/0091-7613(2001)029<0907:SIMPAI>2.0.CO;2**

Torres, M.E., Bohrmann, G., and Suess, E., 1996. Authigenic barites and fluxes of barium associated with fluid seeps in the Peru subduction zone. *Earth Planet. Sci. Lett.,* 144(3–4):469–481. **doi:10.1016/S0012-821X(96)00163-X**

Torres, M.E., Brumsack, H.-J., Bohrmann, G., and Emeis, K.C., 1996. Barite fronts in continental margin sediments: a new look at barium remobilization in the zone of sulfate reduction and formation of heavy barites in diagenetic fronts. *Chem. Geol.,* 127(1–3):125–139. **doi:10.1016/0009-2541(95)00090-9**

Vannucchi, P., Ranero, C.R., Galeotti, S., Straub, S.M., Scholl, D.W., and McDougall-Ried, K., 2003. Fast rates of subduction erosion along the Costa Rica Pacific margin: implications for nonsteady rates of crustal recycling at subduction zones. *J. Geophys. Res.,* 108(B11):2511. **doi:10.1029/2002JB002207**

Vannucchi, P., Scholl, D.W., Meschede, M., and McDougall-Reid, K., 2001. Tectonic erosion and consequent collapse of the Pacific margin of Costa Rica: combined implications from ODP Leg 170, seismic offshore data, and regional geology of the Nicoya Peninsula. *Tectonics,* 20(5):649–668. **doi:10.1029/2000TC001223**

Vannucchi, P., and Tobin, H., 2000. Deformation structures and implications for fluid flow at the Costa Rica convergent margin, Ocean Drilling Program Sites 1040 and 1043, Leg 170. *J. Struct. Geol.,* 22(8):1087–1103. **doi:10.1016/S0191-8141(00)00027-4**

von Huene, R., Ranero, C.R., Weinrebe, W., and Hinz, K., 2000. Quaternary convergent margin tectonics of Costa Rica, segmentation of the Cocos plate, and Central American volcanism. *Tectonics,* 19(2):314–334. **doi:10.1029/1999TC001143**

von Huene, R., and Scholl, D.W., 1991. Observations at convergent margins concerning sediment subduction, subduction erosion, and the growth of the continental crust. *Rev. Geophys.,* 29:279–316.

Walther, C.H.E., Flueh, E.R., Ranero, C.R., von Huene, R., and Strauch, W., 2000. Crustal structure across the Pacific margin of Nicaragua: evidence for ophiolitic

basement and a shallow mantle sliver. *Geophys. J. Int.,* 141(3):759–777. **doi:10.1046/j.1365-246x.2000.00134.x**

White, L.D., 2001. Diatom biostratigraphy of Sites 1039–1043, Costa Rica margin. *In* Silver, E.A., Kimura, G., Blum, P., and Shipley, T.H. (Eds.), *Proc. ODP, Sci. Results,* 170, 1–22 [CD-ROM]. Available from: Ocean Drilling Program, Texas A&M University, College Station TX 77845-9547, USA. [**HTML**]

White, W.M., McBirney, A.R., and Duncan, R.A., 1993. Petrology and geochemistry of the Galápagos Islands: portrait of a pathological mantle plume. *J. Geophys. Res.,* 98:19533–19563.

Wilson, D.S., 1996. Fastest known spreading on the Miocene Cocos–Pacific plate boundary. *Geophys. Res. Lett.,* 23(21):3003–3006. **doi:10.1029/96GL02893**

Wilson, D.S., Teagle, D.A.H., Acton, G.D., 2003. *Proc. ODP, Init. Repts.,* 206: College Station, TX (Ocean Drilling Program). **doi:10.2973/odp.proc.ir.206.2003**

Woodruff, F., and Savin, S.M., 1991. Mid-Miocene isotope stratigraphy in the deep-sea: high resolution correlations, paleoclimatic cycles, and sediment preservation. *Paleoceanography,* 6:755–806.

Zimmer, M.M., Fischer, T.P., Hilton, D.R., Alvarado, G.E., Sharp, Z.D., and Walker, J.A., 2004. Nitrogen systematics and gas fluxes of subduction zones: insights from Costa Rica arc volatiles. *Geochem., Geophys., Geosyst.,* 5(5):Q05J11. **doi:10.1029/2003GC000651**

Zindler, A., and Hart, S., 1986. Chemical geodynamics. *Annu. Rev. Earth Planet. Sci.,* 14:493–571. **doi:10.1146/annurev.ea.14.050186.002425**

Figure F1. Bathymetric map of the eastern central Pacific showing the location of the Leg 205 drilling area in the Middle America Trench offshore Costa Rica. White box shows the location of the map in Figure F2, p. 39. The white circle denotes the location of the Leg 206 site (Wilson, Teagle, Acton, et al., 2003). The map is modified after Vannucchi et al. (2003) based on a data compilation of C. Ranero. Paleolocation of Site 1253 at ~14.5 Ma is shown, following Dreyer et al. (this volume) (from Morris, Villinger, Klaus, et al., 2003).

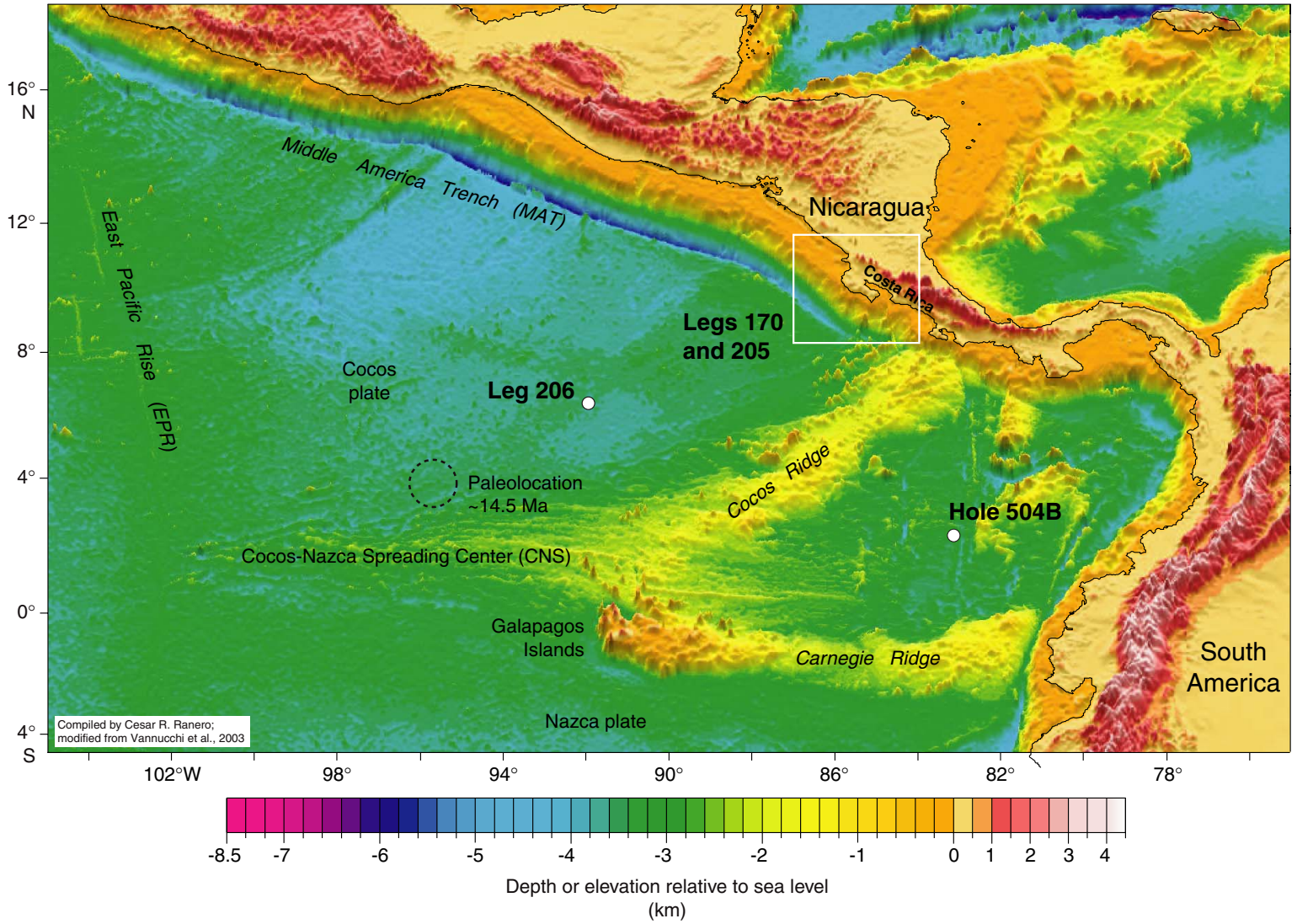

Figure F2. Bathymetric map of the Middle America Trench offshore the Nicoya Peninsula, Costa Rica. White box shows the location of the Leg 205 drilling area. Bathymetry is from Hydrosweep (Ranero and von Huene, 2000) and Simrad (E. Flueh, pers. comm., 2002) swath mapping data combined with ETOPO5. Note position of Fisher Seamount (from Morris, Villinger, Klaus, et al., 2003).

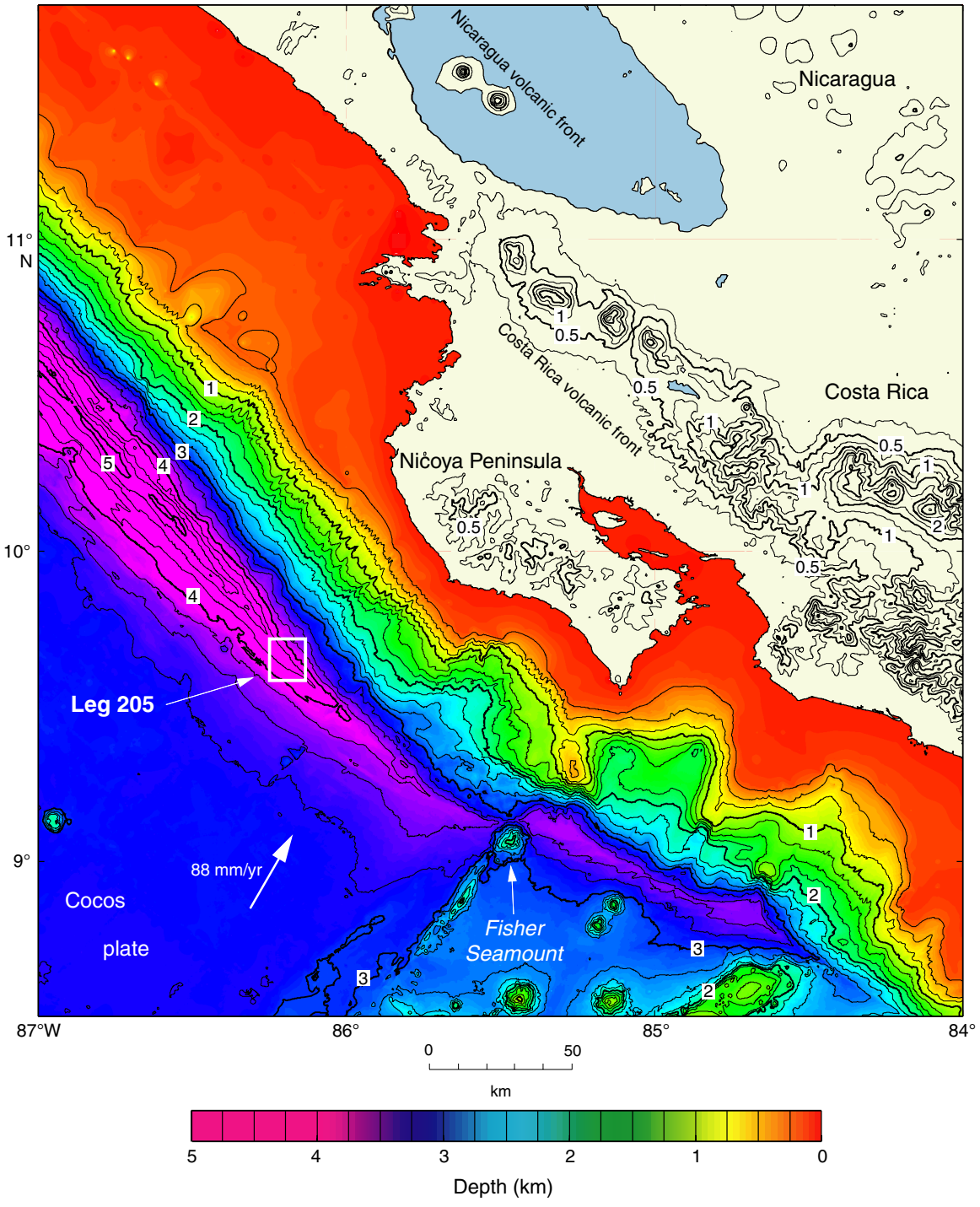

Figure F3. Summary of recovered lithology at drill sites on the incoming plate offshore Guatemala (Deep Sea Drilling Project Site 495) and Costa Rica (Site 1039) as well as on the Costa Rica margin (Sites 1040 and 1043). Note the similarity of incoming sediment sections at Sites 1039 and 495, as well as the repetition of the Site 1039 section below the décollement at Sites 1040 and 1043. Lithologic columns are modified from Kimura, Silver, Blum, et al. (1997). Leg 205 coring at Site 1253 penetrated from ~370 to 600 mbsf, encountering the sill seen in Leg 170 sites, underlain by a thin layer of sediments and a deeper igneous section. At Site 1254, coring was carried out in the intervals 150–223 and 300–370 mbsf, encountering the lithologies and structures seen at Site 1040. At Site 1255, coring was restricted to the décollement zone (from Morris, Villinger, Klaus, et al., 2003).

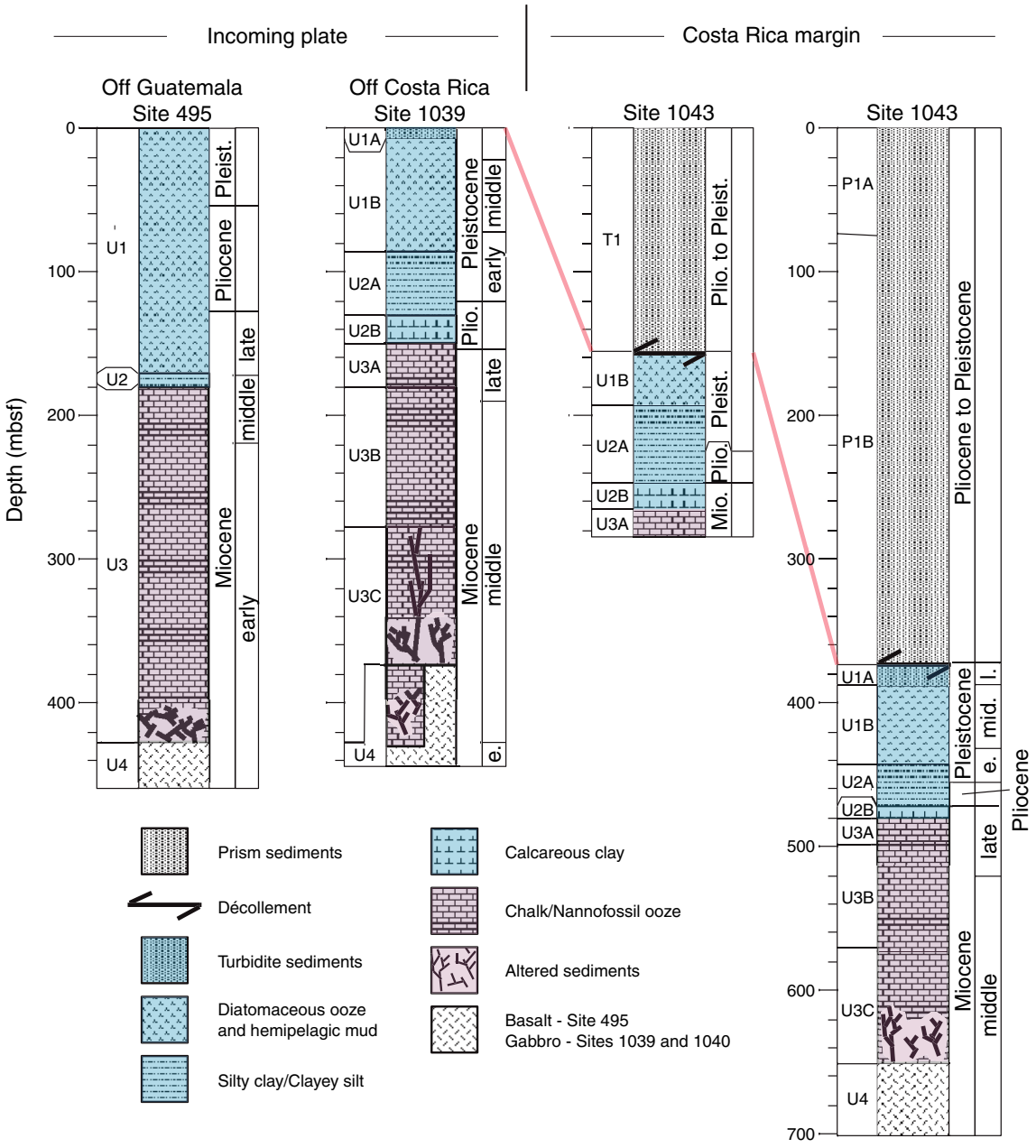

Figure F4. Leg 205 Costa Rica drilling area (box) and isochrons derived from seafloor magnetic anomalies (Barckhausen et al., 2001). Numbers indicate crustal age in millions of years. Tectonic boundaries, convergence direction and rate (arrow) (DeMets et al., 1990), and arc volcanoes (triangles) are shown. QSC = Quesada Sharp Contortion. Dashed ellipse encloses proposed region of sill intrusion from Silver et al. (2004). Note transition from rough to smooth incoming crust, following Hey (1977), and "seamount" region (from Morris, Villinger, Klaus, et al., 2003).

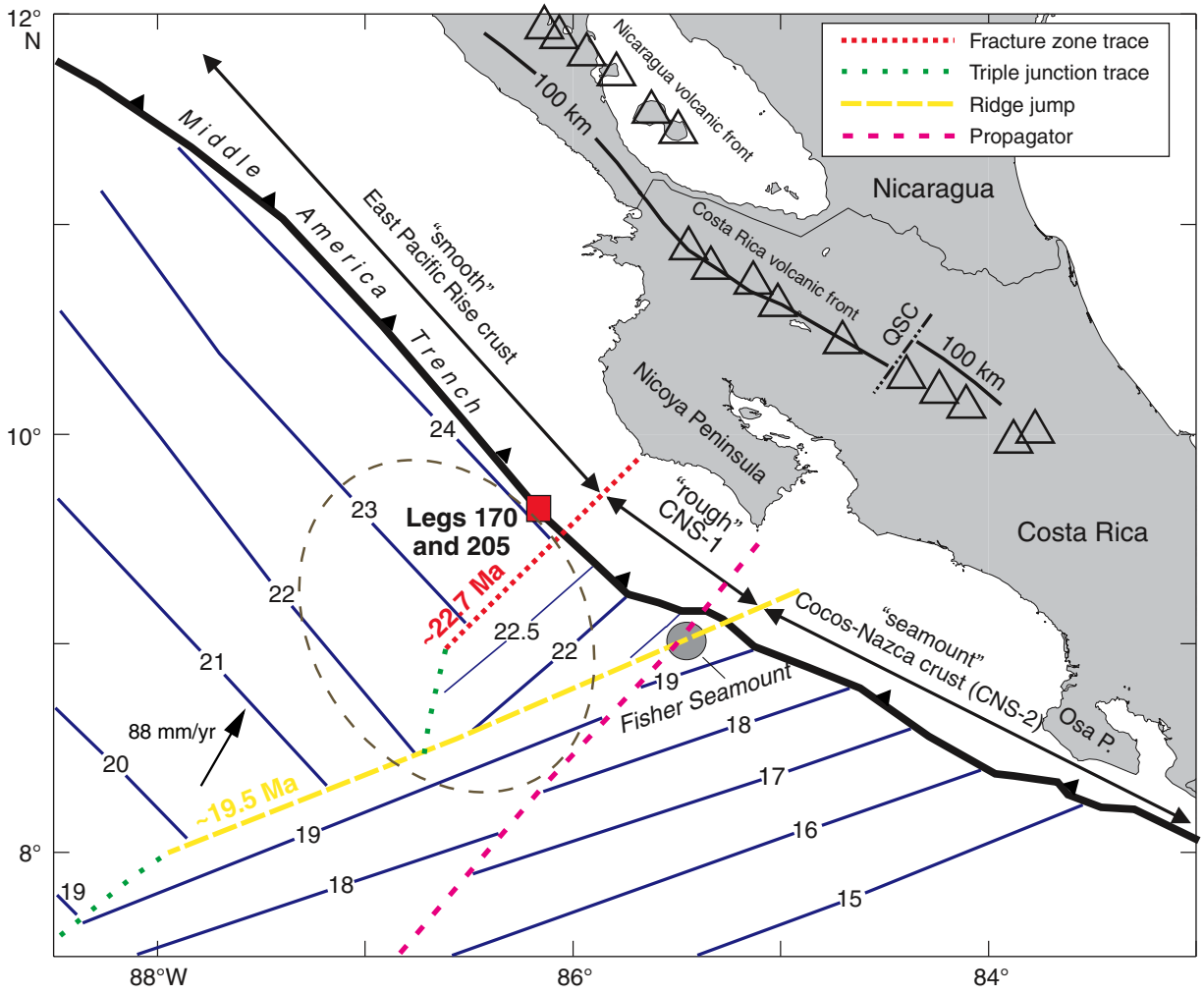

Figure F5. Migrated multichannel seismic Profile BGR-99-44 (C. Ranero and C. Reichert, pers. comm., 2001) across the Middle America Trench. Thick lines = Leg 205 Sites 1253, 1254, and 1255. Thin lines = Site 1039, 1040, and 1043 (Leg 170) locations (Kimura, Silver, Blum, et al., 1997). CMP = common midpoint. (Figure from Morris, Villinger, Klaus, et al., 2003).

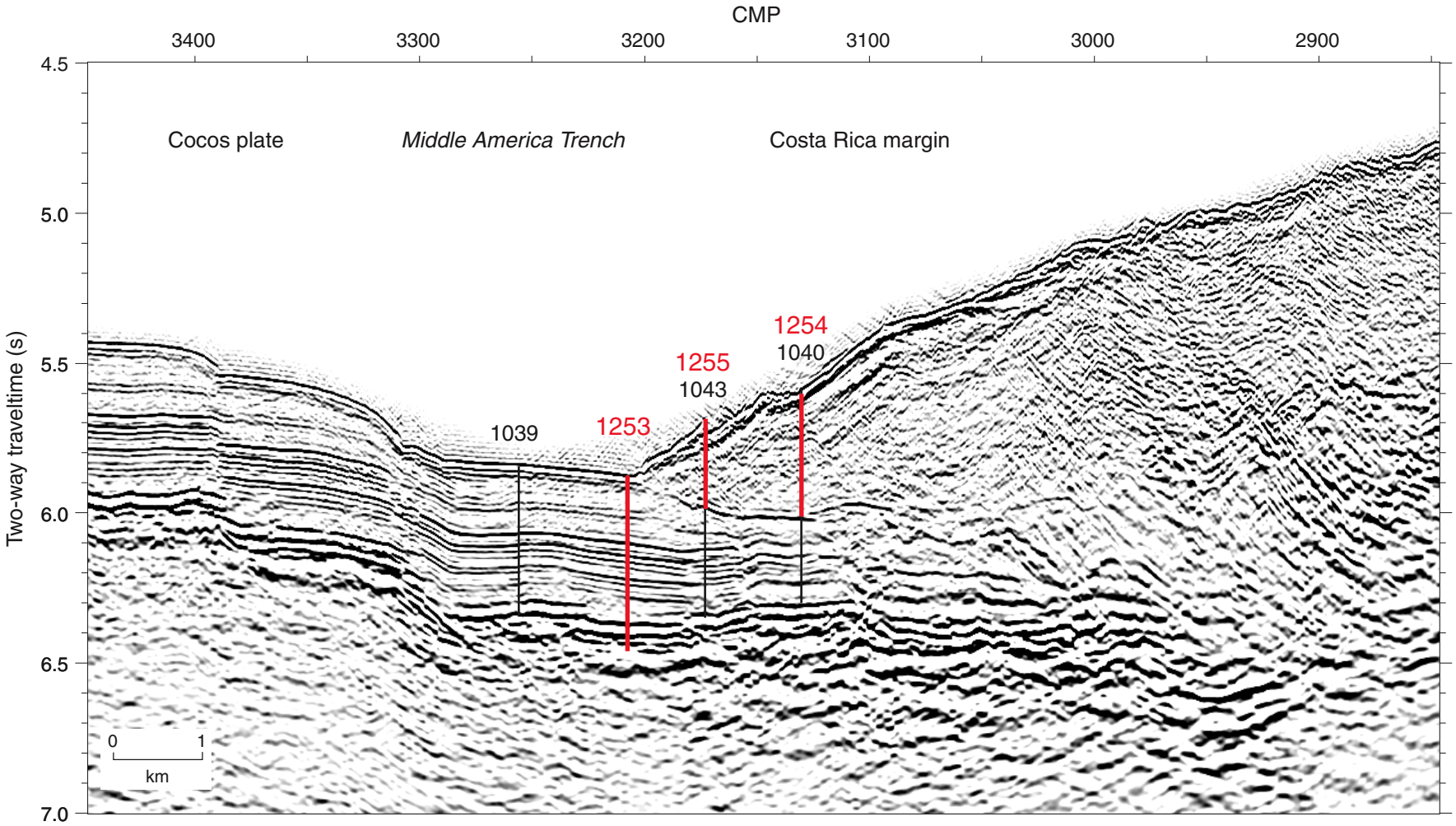

Figure F6. Composition of pore fluids squeezed from carbonates at the base of Site 1039. Strontium isotope ratios from pore waters are indicated by data points and solid line in left panel; dashed line shows the strontium paleoseawater mapped onto the age-depth profile of the sediments. Note that basal pore water trend toward modern seawater composition, with values greater than Miocene seawater, indicating a strong modern seawater component in basement fluids. Similar variations are seen in calcium and strontium concentration data. Pore water chemical profiles from basal sediments at Site 1253 show the same patterns for these and additional tracers (see fig. F20 in Shipboard Scientific Party, 2003).

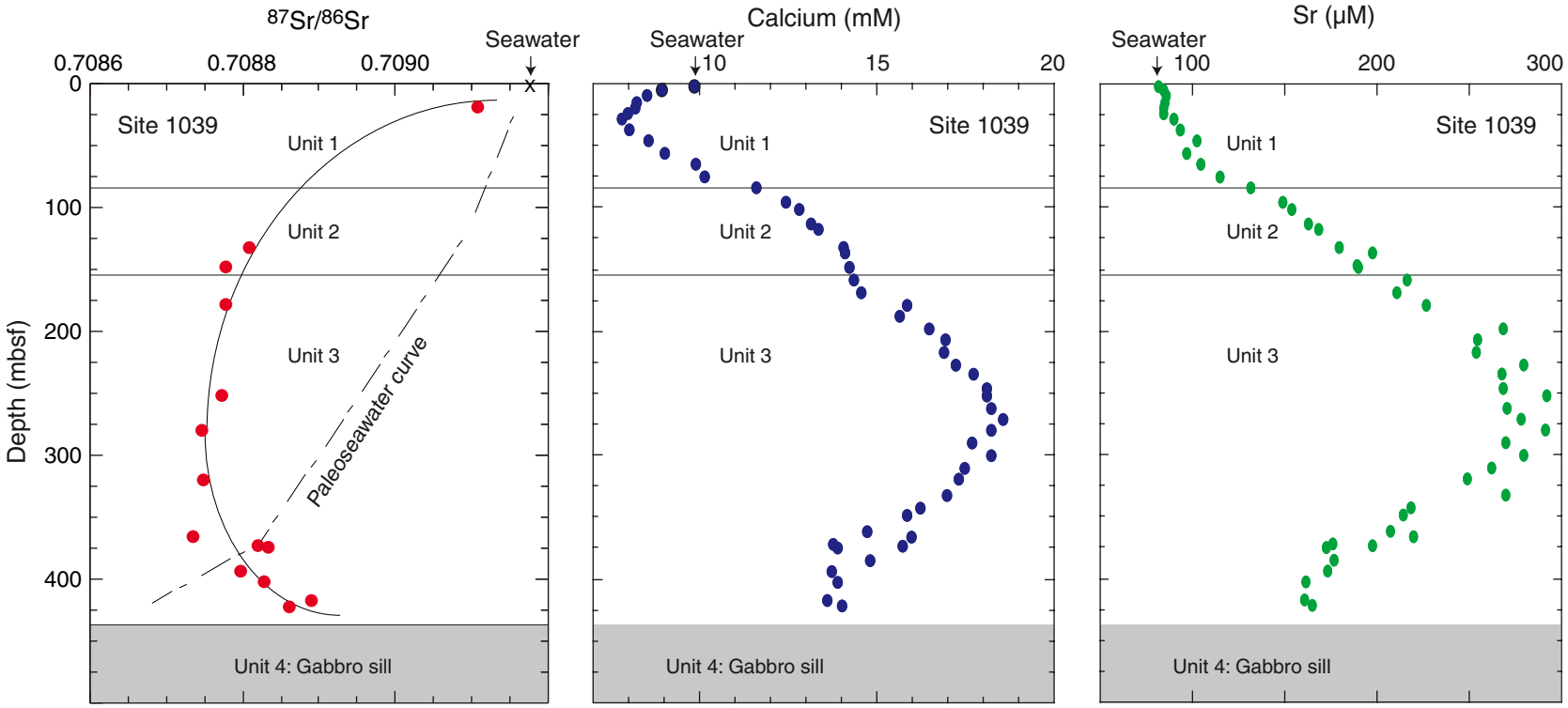

Figure F7. Structures and geochemical anomalies in Hole 1040A, compiled from Kimura, Silver, Blum, et al. (1997) and Silver et al. (2000). Note anomalies in pore fluid chemistry in fault zones and décollement, along with sharp contrast between pore fluid chemistry in the underthrust sediments and in the décollement zone. Similar anomalies are seen in results from Sites 1254 and 1255 (**Kastner et al.,** this volume; see also fig. F10 in Shipboard Scientific Party, 2003).

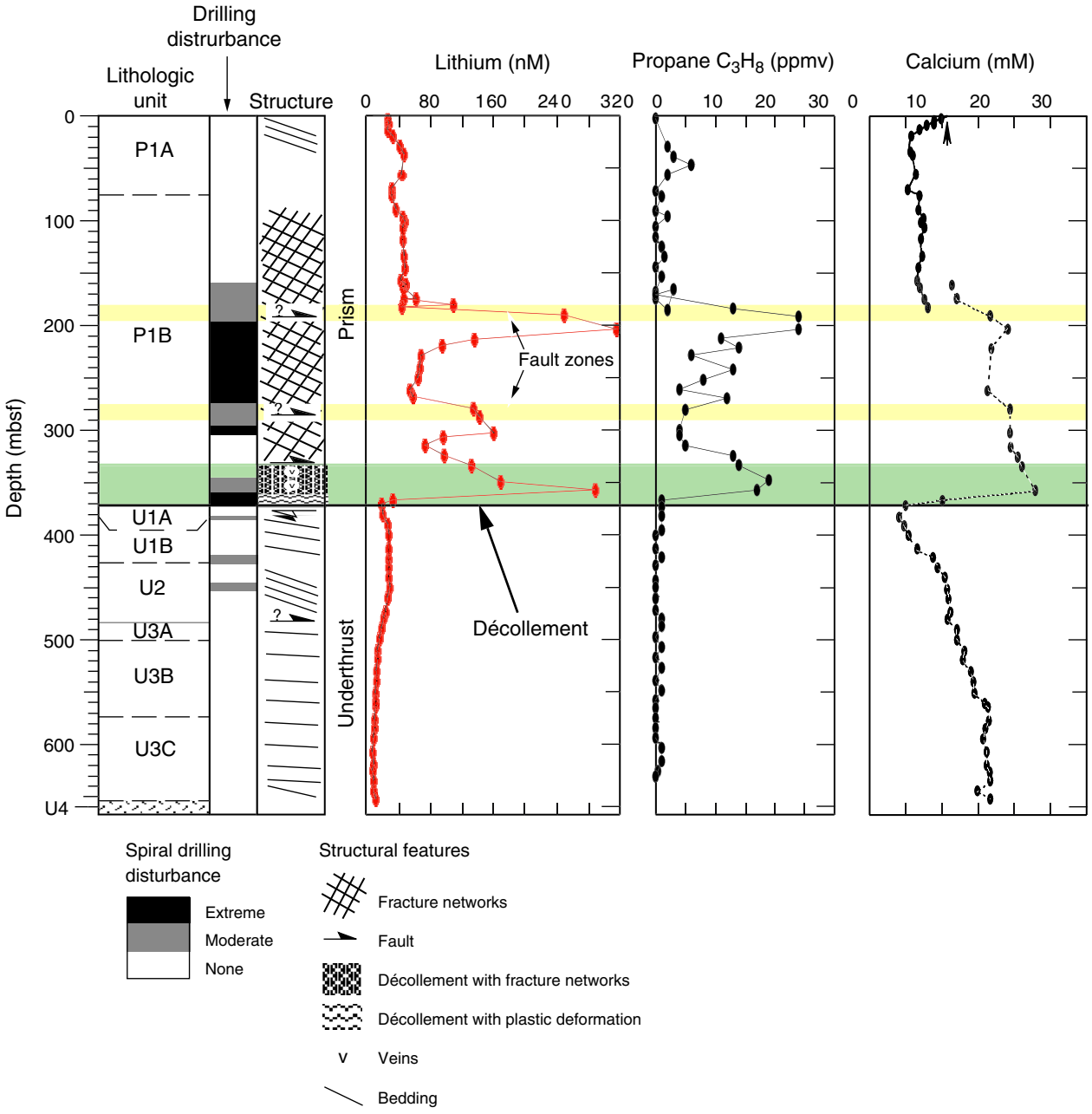

Figure F8. Schematic for Hole 1253A borehole installation, showing subseafloor depths for two OsmoSamplers, screens, packers, and casing strings. Note that figure is not to scale. Pressure monitoring screens are located just above packer (located within igneous Subunit 4B-2) and within sampling screen. Miniaturized temperature loggers are housed in each OsmoSampler package, located within igneous Subunits 4B-4 and 4B-5, respectively. Hole is open beneath the packer to depth of 600 mbsf (from fig. F21 in Shipboard Scientific Party, 2003). ROV = remotely operated vehicle, RCB = rotary core barrel.

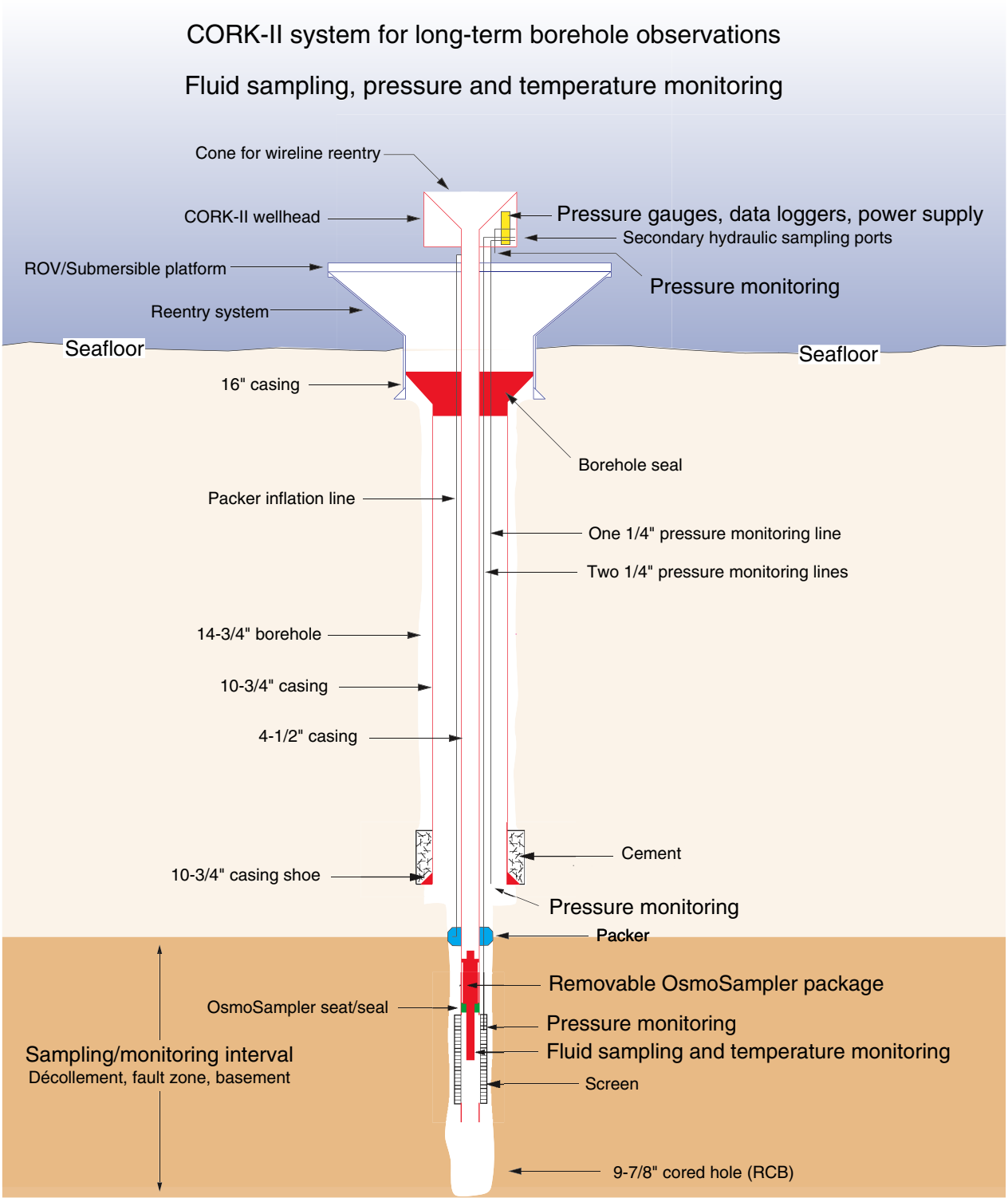

Figure F9. Schematic for Hole 1255A borehole installation, showing subseafloor depths for one OsmoSamplers, screens, packers, and casing strings. Note that this figure is not to scale. Pressure monitoring screens are located just above packer (located within basal prism sediments) and within sampling screen. Miniaturized temperature loggers are housed in the OsmoSampler package, situated within décollement zone. Hole terminates at 153 mbsf, immediately below instrumented horizon (from fig. F30, Shipboard Scientific Party, 2003).

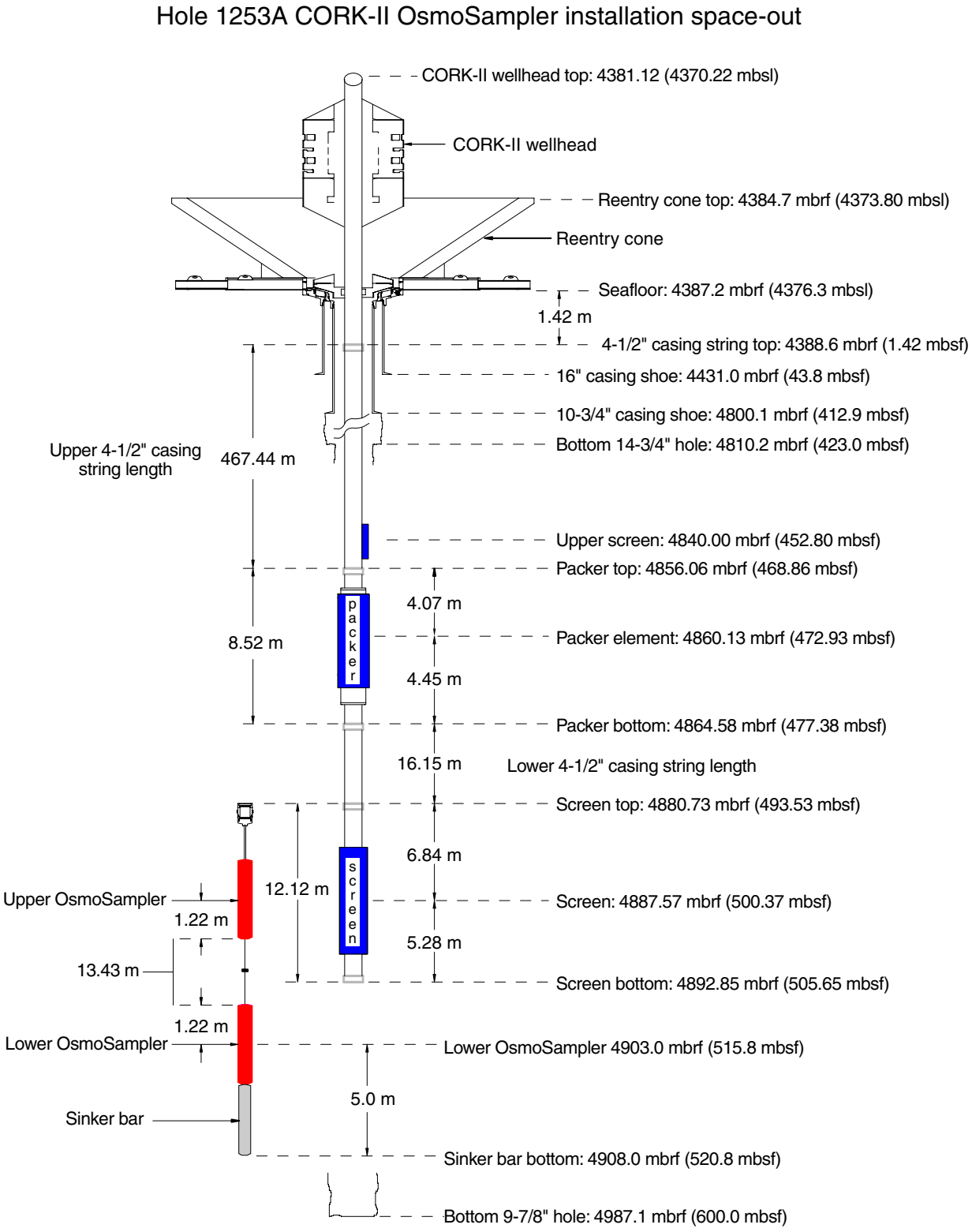

Figure F10. Core recovery plot for Hole 1253A from 370 to 600 mbsf (line), superimposed on summary of petrologic observations. Diagram shows multiple distinct intervals within Subunit 4A, the gabbro sill, and Subunit 4B. Different shaded areas indicate the following observations. 1 = location of the cryptocrystalline basaltic texture, 2 = higher number of magmatic contacts, 3 = more veins or voids filled with holocrystalline and cryptocrystalline groundmass/altered glass, clay, and zeolites, 4 = up to 5% degree of alteration within 1 m of Section 205-1253A-37R-1 and higher abundance of voids filled with clays and zeolites ending in a homogeneous microcrystalline gabbro, 5 = increasing number of centimeter-scale fractures and veins, 6 = very homogeneous microcrystalline to fine-grained gabbro with very weak magmatic contacts. Also indicated are the positions of the two OsmoSamplers (OS).

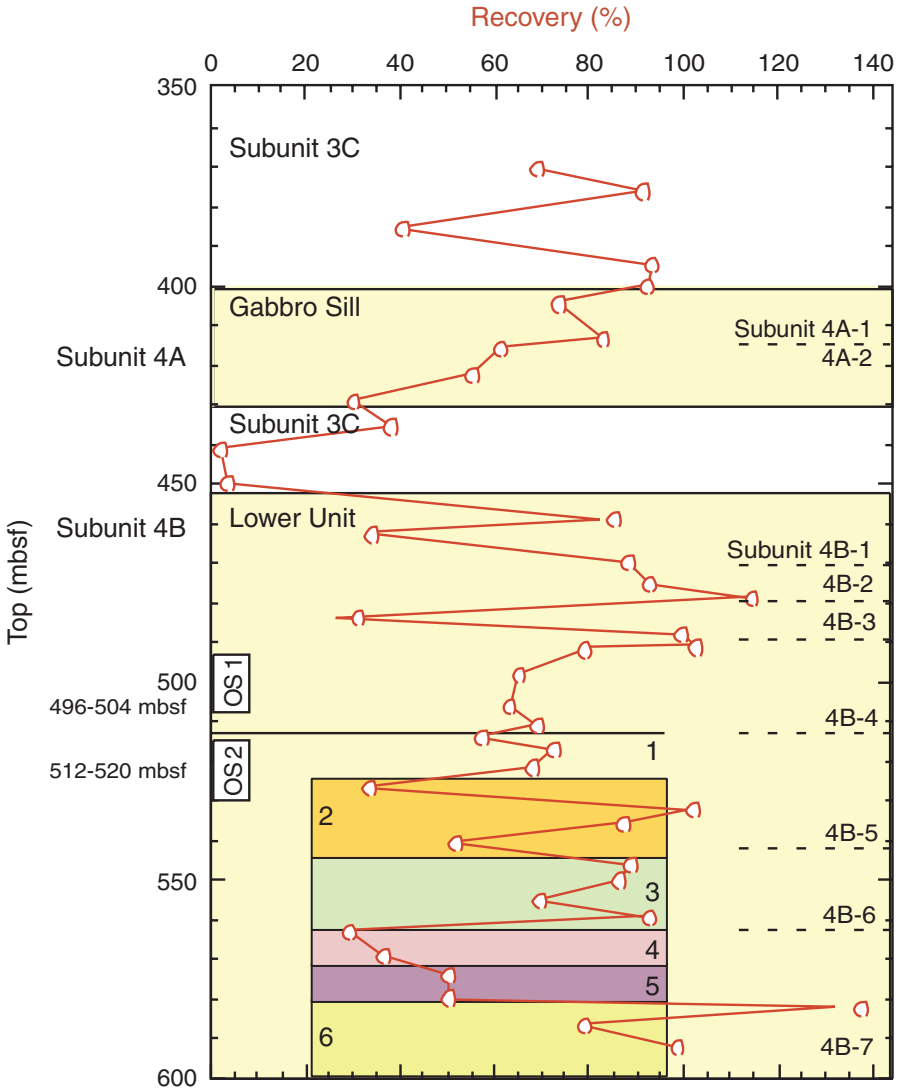

Figure F11. Composite diagram showing fracture distribution based on Formation MicroScanner (FMS) data and core observations, along with estimates of Stoneley energy and borehole diameter (from **Pfender and Villinger,** this volume). OsmoSamplers (OS) 1 and 2 were located at 497–504 mbsf and 512–519 mbsf, respectively.

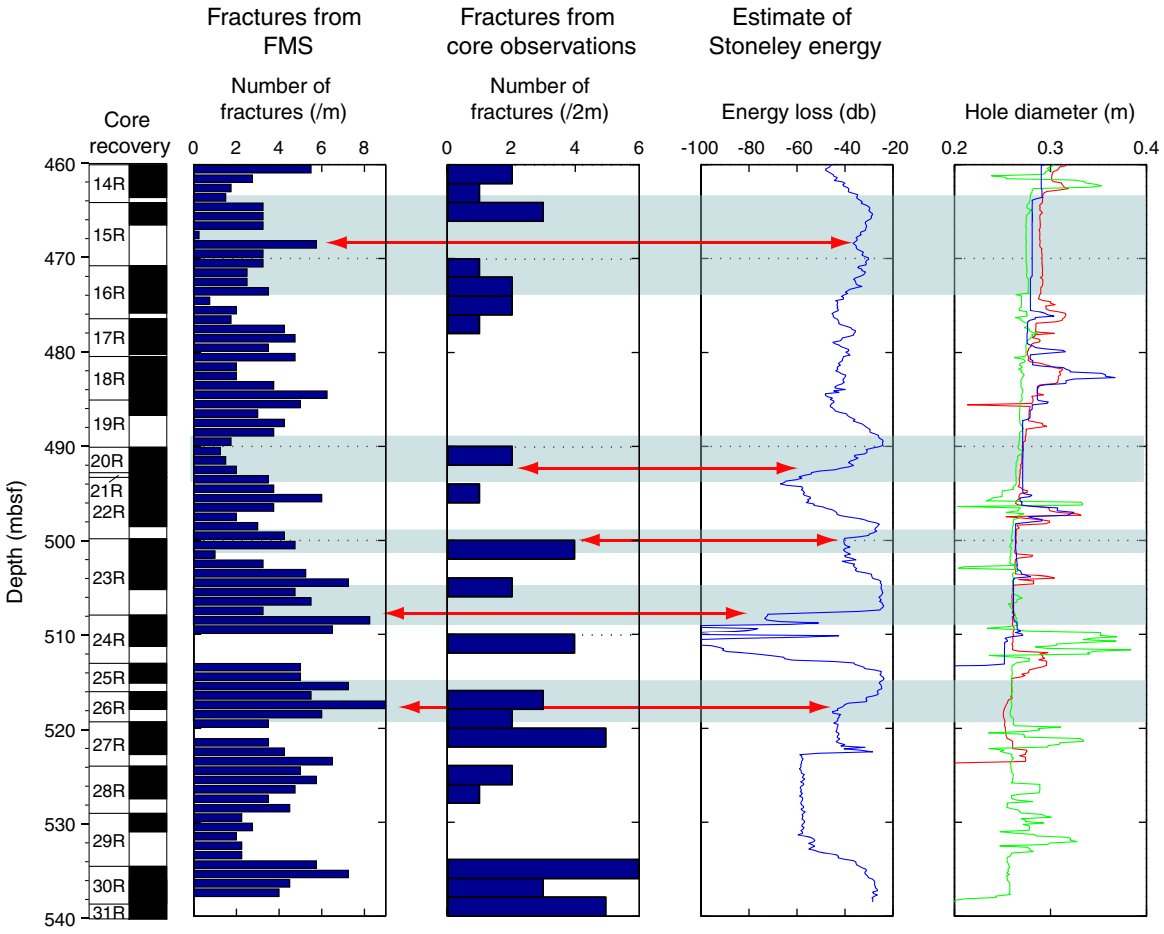

Figure F12. Sr isotope stratigraphy of igneous rocks (bulk rock) at Site 1253, from Chavagnac (pers. comm., 2005) and Dreyer et al. (2005). Excursions to high $^{87}Sr/^{86}Sr$, indicative of seawater alteration, are generally observed over limited depth horizons at petrologically defined boundaries between igneous subunits. Arrows labeled N-MORB (normal mid-ocean-ridge basalt) and OIB (ocean island basalt) indicate peak values in histograms showing range of observed isotopic variation in lavas erupted in the two settings (Zindler and Hart, 1986).

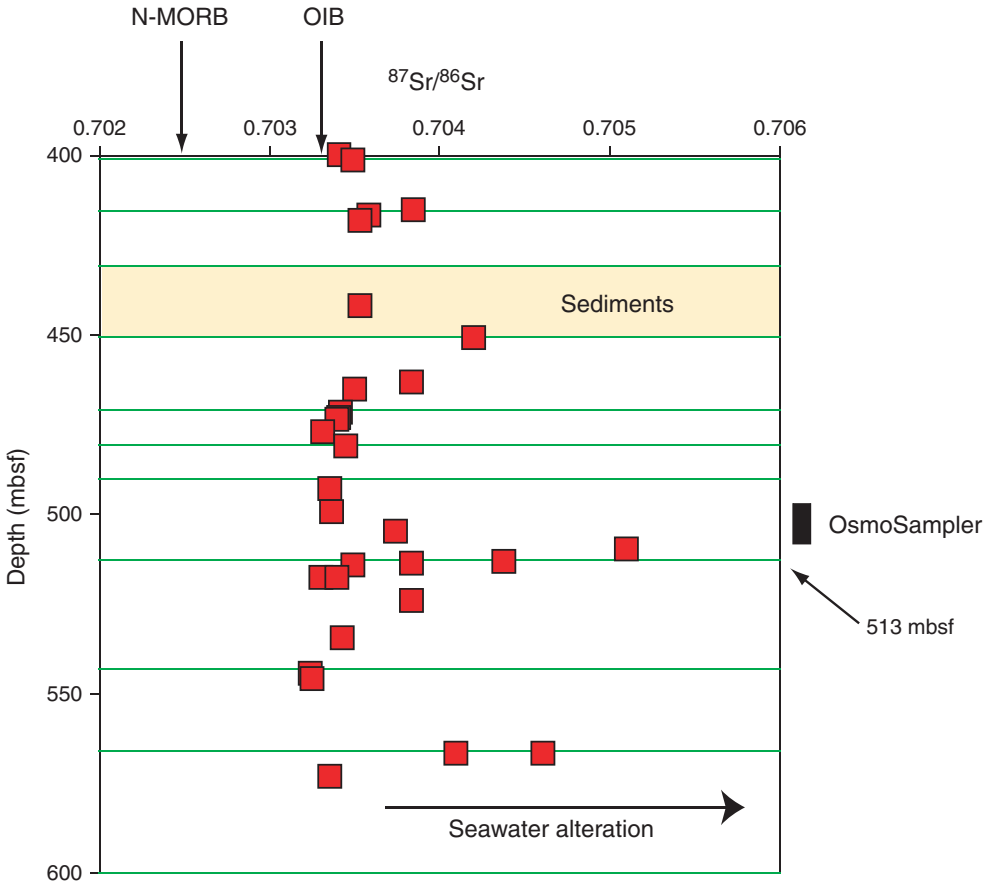

Figure F13. Bulk sediment $\delta^{13}C$ from Leg 170 Site 1039 (from **Strasser et al.,** this volume). Record is correlated to mid-Miocene records from a pelagic section at DSDP Site 574, equatorial Pacific (Woodruff and Savin, 1991) and an outcrop section on Malta (John et al., 2003). See text and **Strasser et al.** (this volume) for explanation. VPDB = Vienna Peedee belemnite.

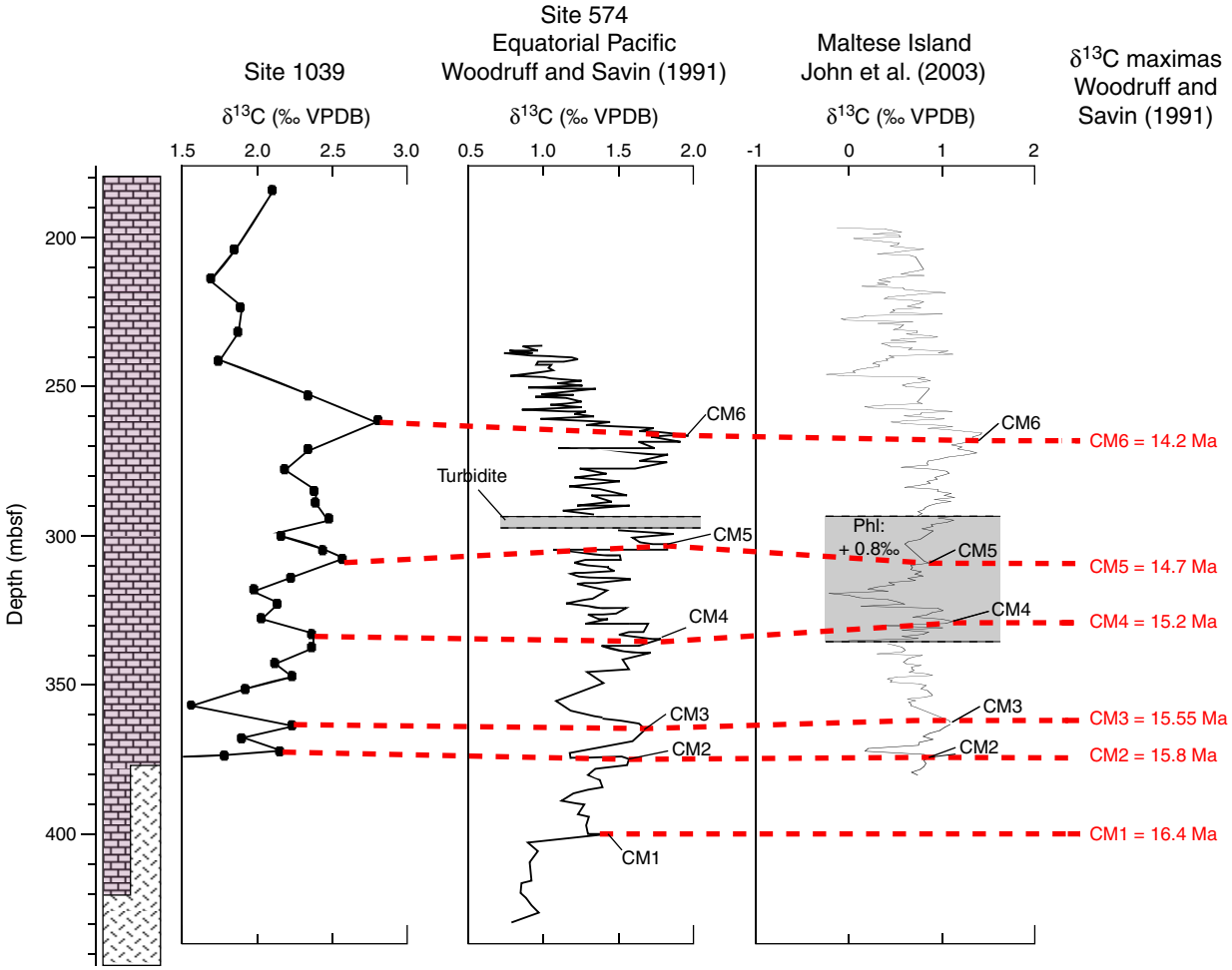

Figure F14. Plots of pore fluid Ba and sulfate concentration vs. depth (from **Solomon et al.,** this volume). **A, C.** Site 1039/1253. **B, D.** Site 1040/1254. UFZ = upper fault zone. Units U1–U3 and P2 refer to stratigraphic units shown in Figure **F3,** p. 40. ICP-OES = inductively coupled plasma–optical emission spectrometry, ICP-MS = inductively coupled plasma–mass spectrometry. SW = seawater, BW = bottom water.#

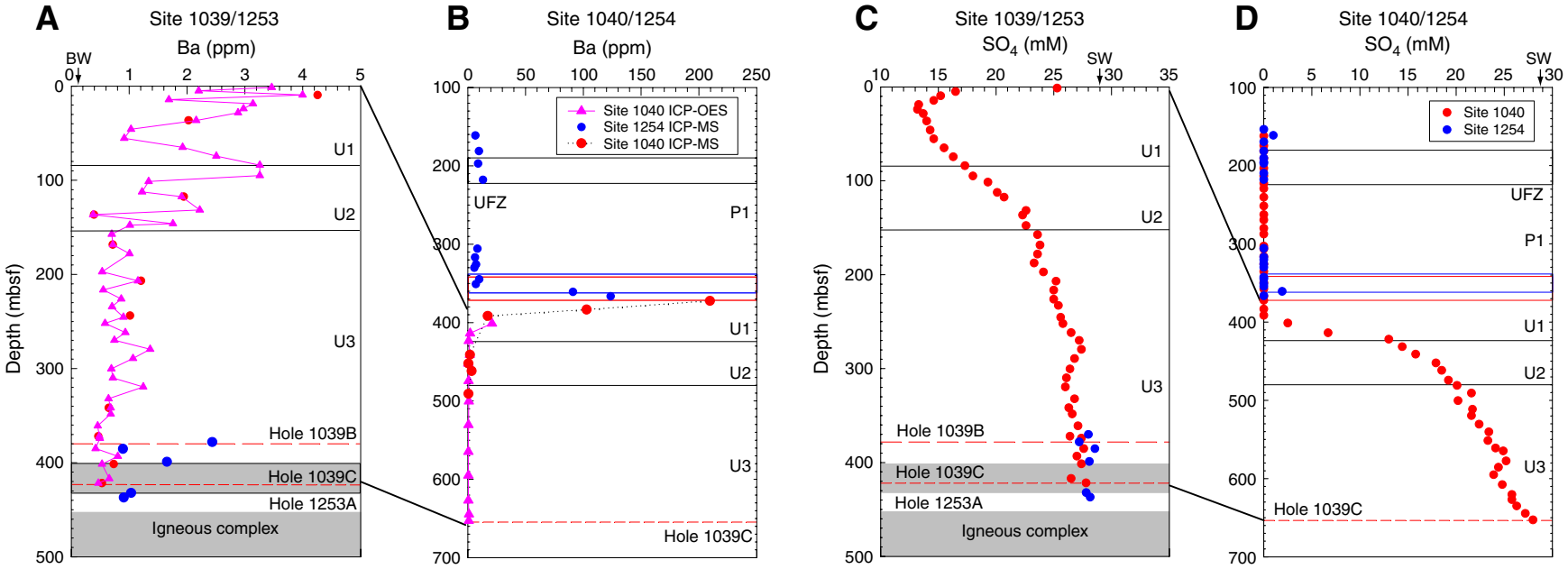

Figure F15. **A, B.** Pressure and temperature variations at Site 1253, following Davis and Villinger (2006). **C.** Ca and Mg concentration variations through time in formation fluids collected by OsmoSampler 1 from Kastner et al. (2005). Note abrupt change in composition when borehole was temporarily open to seawater during the attempted instrument recovery in March 2004. UTC = Universal Time Coordinated.

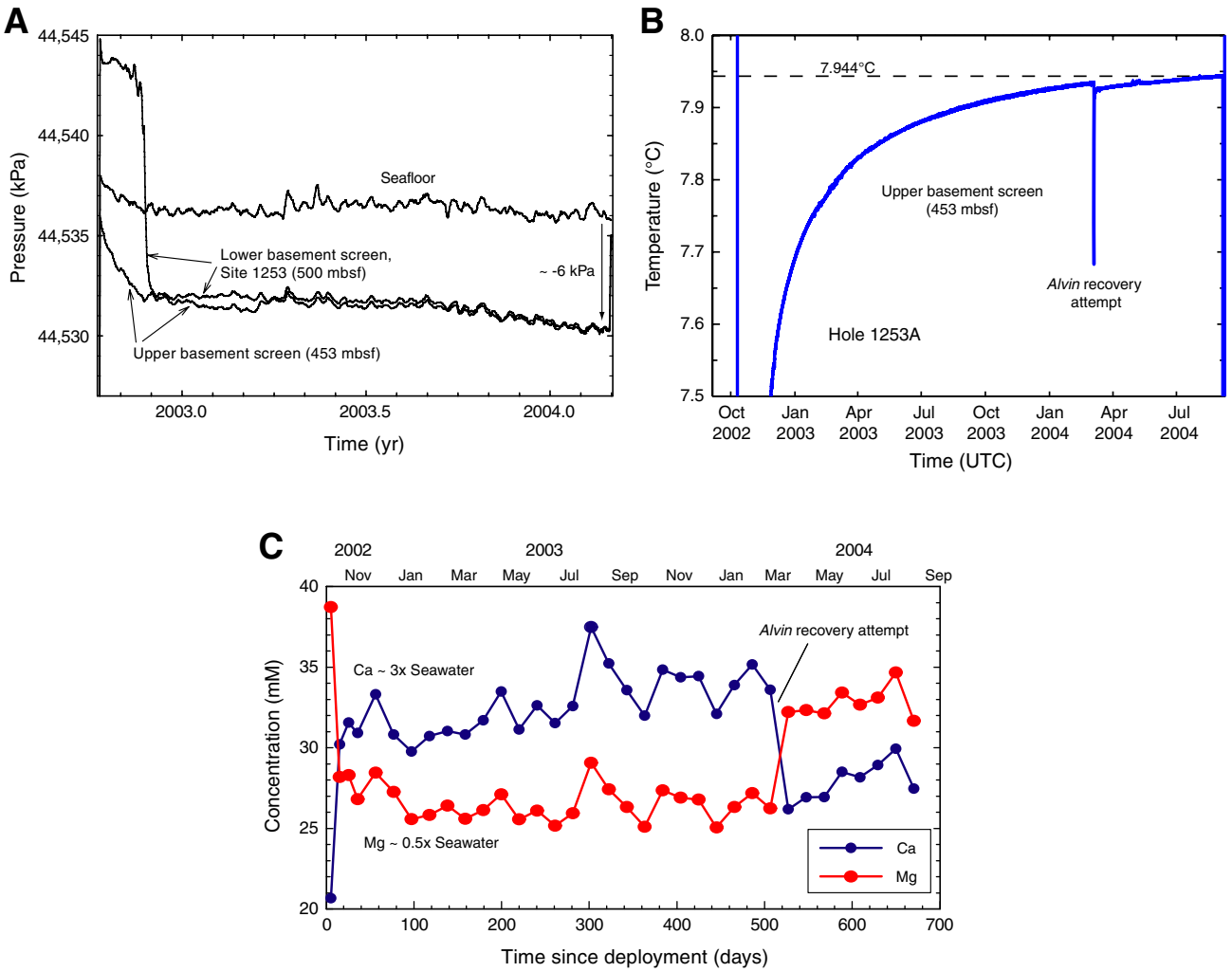

Figure F16. Pressure variations measured at Site 1255 in the upper screen (in prism sediments) and the lower screen, within the décollement, along with results of coastal Global Positioning System (GPS) monitoring, from Protti et al. (2004) (modified from Davis and Villinger, 2006).

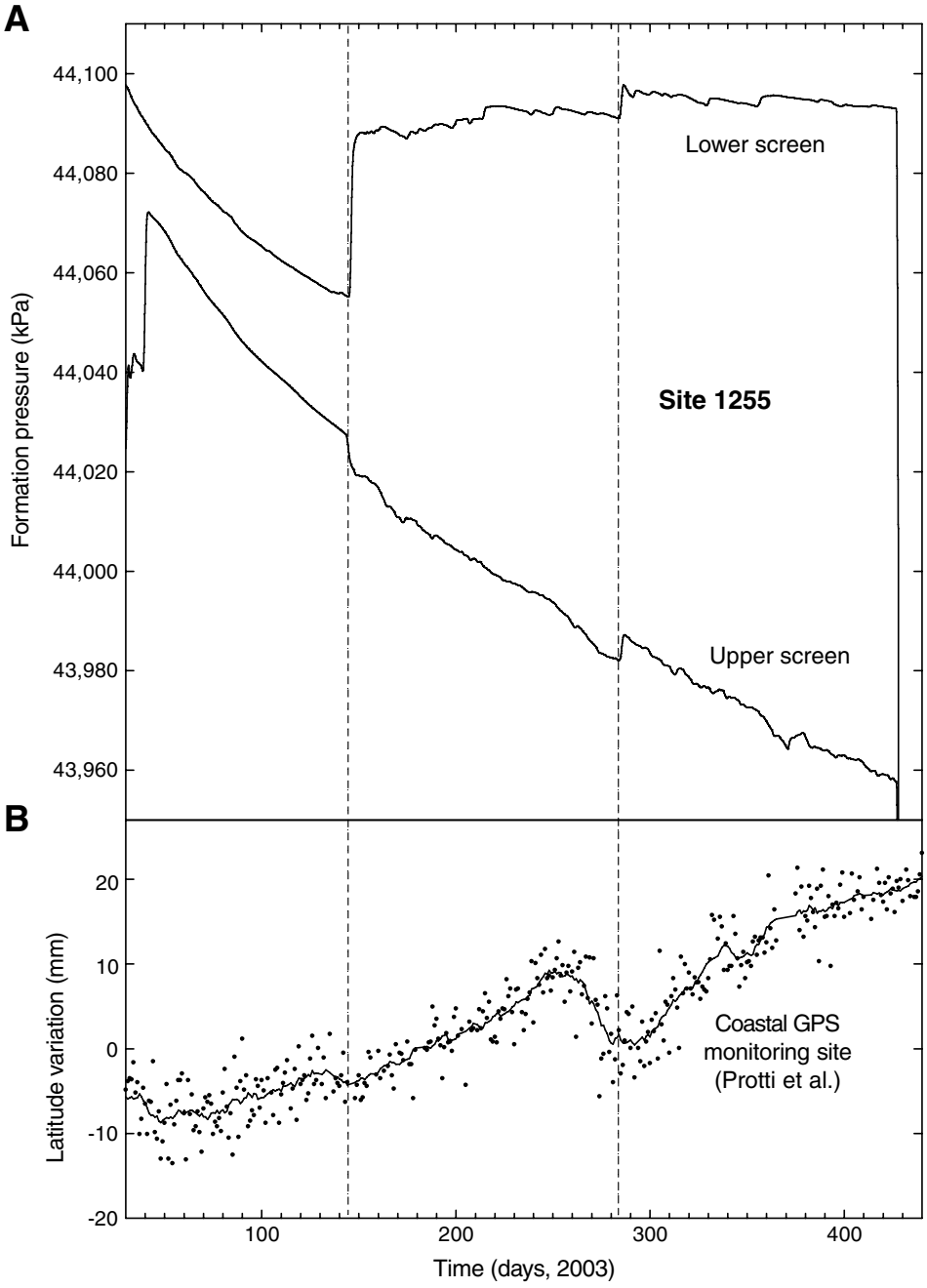

Figure F17. Ammonium concentration variation through time in formation fluids collected by OsmoSampler within the décollement at Site 1255 (Kastner et al., 2005). Events 1 and 2 refer to those shown in Figure F15, p. 52; note that excursions in chemistry correspond to pressure and temperature excursions.